EFFECT OF ELASTIC DEFORMATIONS ON THE CAPACITY OF LATERALLY LOADED CAISSONS

A Thesis

by

CHUHAO LIU

Submitted to the Office of Graduate and Professional Studies of
Texas A&M University
in partial fulfillment of the requirements for the degree of

MASTER OF SCIENCE

Chair of Committee,	Charles P. Aubeny
Committee Members,	Robert L. Lytton
	Jerome J. Schubert
Head of Department,	Robin Autenrieth

May 2017

Major Subject: Civil Engineering

ABSTRACT

Suction caissons are one of the most common anchoring systems used in offshore foundations. With increasing exploration in offshore energy, it becomes important to do research on suction caissons.

The purpose of this study is to investigate the elastic behavior of suction caissons. A 3D finite element simulation is used for this purpose and performed in ABAQUS. In order to enhance accuracy of simulation elastic deformation of caissons, calibration factors are calculated by comparing displacements from simulations and the theoretical solution. The parametric study is conducted for three parameters, which are thickness, load attachment location, and soil strength profile. The surrounding soils is transformed into springs by extracting nodal forces and displacement of caissons. The spring properties are compared with these from previous research, which obtains spring properties from a 2D model.

Results show that the effect of caissons' elastic behavior on capacity is different with that of caisson's rigid behavior. Also, the spring properties in this study are different from those in other research.

ACKNOWLEDGEMENTS

First of all, I would like to thank my committee chair, Dr. Aubeny. Without his guiding, it is impossible for me to achieve simulation result so quickly and successfully. I also would like to thank my committee members, Dr. Lytton and Dr. Schubert. They gave me many good suggestions to help me improve my thesis.

Secondly, I would like to thank my mentor, Francisco. He taught me everything about this research in details. I learned how to run ABAQUS efficiently from his experiences. It is indeed a good time to work with him.

Lastly, I would like to thank me friends. Shuna helped me a lot on fixing bugs occurred in ABAQUS. Her advice saved me a lot of time on fixing program peoblem. I would thank Mark, my colleague, for accompanying me every work day. He always can give me a good mood, which makes me work efficiently. Also, I would like to thank my family for supporting me during these two years. Without their support, I could not have met so many distinguished professors and good friends.

CONTRIBUTORS AND FUNDING SOURCES

Contributors

This work was supervised by a thesis committee consisting of Professor Charles Aubeny and Professor Robert Lytton of the Department of Civil Engineering and Professor Jerome Schubert of the Department of Petroleum Engineering.

The FEM model used in section 4 was provided by Professor Charles Aubeny and fellow colleague Francisco Grajales. The method used in section 5 was provided by Dr. Yuze Zhang. All other work conducted for the thesis was completed by the student under the advisement of Professor Charles Aubeny, fellow colleague Francisco Grajales and Shuna Ni.

Funding Sources

This work was completed without outside financial support.

TABLE OF CONTENTS

Page

LIST OF FIGURES

LIST OF TABLES

1. INTRODUCTION

Due to the increasing demanding on the energy, it is becoming necessary to explore the offshore energy, such as oil, gas and wind energy, in a deeper water area. To achieve this goal, the offshore industry has been developing innovative foundations over last 70 years. At first, in the shallow water area, the upper structures are supported by fixed foundations, such as gravity base foundations and jacket foundations (Figure 1.1 (Schneider & Senders, 2010)). The jacket foundations are easy to construct onshore and floated to the destination location. Furthermore, they can be installed in very short time, minimizing the negative effects of weather and waves and thus decreasing the costs. Therefore, by taking advantage of this foundation, higher jackets are built to support upper structures when moving toward deeper water area. By 1970, such jacket foundations had installed in sites up to 200 m in depth.

Although, it is possible to construct larger jacket foundations to deal with the over 200m deep water situation, it is not cost effective to continue using such foundations. The oil&gas industry had developed template structures (less than 450m water depth) and compliant towers (300 to 600m water depth). But they still had the high cost because of the additional materials to construct larger foundations. To minimize this disadvantage in the fixed structures, the oil & gas industry developed the floating structures in the early 1970s, which can be used in up to 2500m water depth. In this case, the platform is floating at the water surface and fixed by the steel cables tied with the anchors located in the seabed.

The most important part in such system is the anchor founded in the seabed. The upper structures need to be stabilized by the anchors from winds, waves, currents, etc. The suction caissons are one of the most popular anchors used in floating system. Also, this research focus on the capacity of the suction caisson.

1.1 The definition of suction caisson

The suction caisson is a cylindrical foundation, opened at bottom and closed at top, like an upturned bucket (Figure 1.2 (Photo: E.C. Clukey, BP)). The mooring loads are usually applied to it by the steel cables, which are attached at the optimum point of the skirt of the caisson, where the failure mode has the largest translational displacement and minimal rotation (Schneider & Senders, 2010).

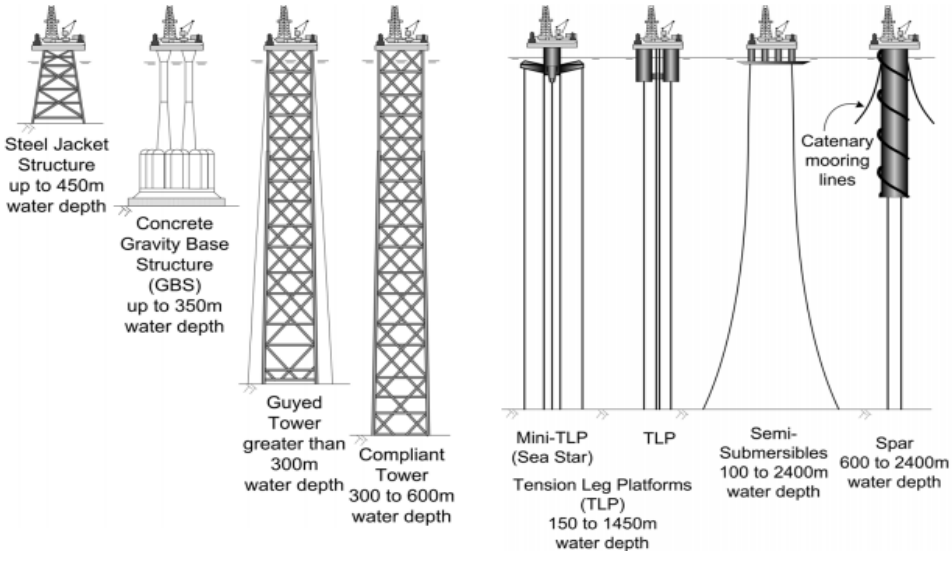

Figure 1.1 Evolution of the offshore substructures. (Schneider & Senders, 2010)

Figure 1.2 Suction caissons in the Gulf of Mexico. (Photo: E.C. Clukey, BP)

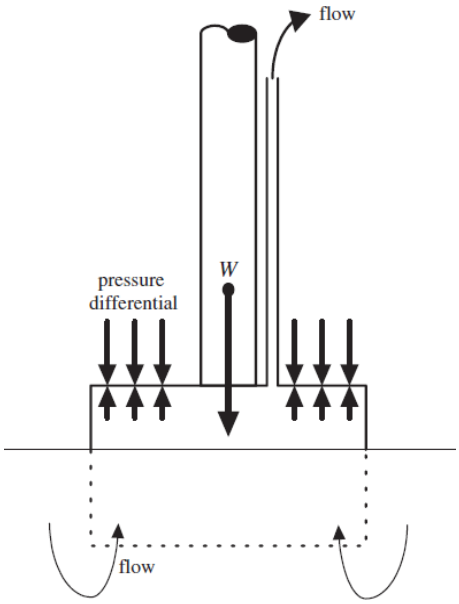

Figure 1.3 Suction installation (Byrne, B.W. and Houlsby, G.T., 2003)

The typical length to diameter ratio is around six or less. There are two steps when installing the suction caisson. The first step is to penetrate foundation into soil by self-gravity with vent open, which is always not sufficient to load into required depth. The second step is to apply the negative pressure to caisson's interior by extracting the water out through valves. As Figure 1.3 (Byrne, B.W. and Houlsby, G.T., 2003) shows, the differential pressure between inner water pressure and outer water pressure will sink caissons further until to the designed location. After full penetration, the top is sealed off and suction caisson acts like a short pile foundation. The advantage of this type of foundation is that it can be installed very fast with the aid of the suction, especially compared with the piles which need to be installed by hammered into the ground. Also, it

can be extracted easily by reversing the installation procedure. And it can be reused. The capacity of it is also greater than that of embedded anchors. Therefore, this type anchor has been extensively used in the offshore industry. According to Andersen et al (2005), over 485 suction caissons had been installed in more than 50 locations whose water depth was up to 2000m. It had been used in the world's most deep water area, such as Gulf of Mexico.

1.2 Problem description

Although there are numerous researches conducted on the capacity of the suction caissons, few of them have considered the effect of elastic behavior of caissons on the capacity. Usually, researchers consider caisson as a rigid body, as its elastic modulus is very high compared with around soils. However, recent research found out that the elastic behavior of caisson indeed has an effect on the capacity. In addition, the relation of the load-displacement is also received little attention. Therefore, the aim of this research is to investigate the effect of elastic behavior of the caisson on the capacity by 3-D continuum finite element method and compare the result with other methods.

2. LITERATURE REVIEW

Suction caisson is one of the most popular offshore foundations. It has been researched for many years. Many literatures have done a lot of researches on the capacity. Also many literatures have developed a finite element analysis on the suction caisson. Some literatures have also developed spring models to simulate the contacting problem between surrounding soils and caissons.

There are many researches on the capacity of the suction caisson. House and Randolph (2001) have conducted installation and pullout tests of the suction caissons and found that the drained pullout capacity after soaking is far greater than that under immediater monotonic drained pullout. Houlsby et al (2005) conducted many field trials of suction caisson in soft clay under cyclic loading and found the existence of gapping at the side of the caisson and a reduction of stiffness. Andersen et al (2005) compared the calculated capacity from different methods with the result of the 3D finite element method and found that the plane limiting equilibrium method and plastic limit analysis method both gave good results. Vásquez et al (2010) conducted a finite element analysis of the axial capacity of the suction caissons and found that the results of simulation and experiments are in general agreement. However, there are differences in the results of the pore water pressure at the inner, outer caisson walls and the tip, which may be caused by the structural change in the vicinity of the caisson and the insufficient mesh.

Gerolymos and Gazetas (2006) has developed a nonlinear Winkler-spring model to assess the static, cyclic and dynamic behavior of the suction caisson foundation by

simulating nonlinear soil reactions surrounding caissons and at the bottom of caissons with reasonable and realistic translational and rotational nonlinear interaction springs. According to Gerolymos and Gazetas (2006), the springs can capture a lot of realistic phenomenon, which are separation and slippage at the caisson-soil interface, uplift of the caisson base, radiation damping, stiffness and strength degradation with large number of cycles. Also, Gerolymos and Gazetas (2006) has implemented this method in a finite difference time-domain code, NL-CAISSON and calibrated parameter by a numerical methodology with usage of a lot of experimental and analytical data. Gerolymos et al (2006) then validate this model by a in situ medium-scale static load tests and results from 2D finite element analysis.

Bransby and Randolph (1998) has developed a finite-element analysis of a strip footing in undrained soil and a plasticity mechanisms of vertical, horizontal and moment loading. Bransby and Randolph (1998) found that footing displacements obey normality on the yield locus, upper-bound plasticity analysis has a similar yield locus with the finite element analysis, the yield locus is eccentric in H-M space within the maximum moment sustained with a significant amount of horizontal load.

Sukumaran et al (1999) has conducted a finite element analysis by using linear elasticity combined with the von Mises strength model to simulate the soil deformation and typical properties shown in Gulf of Mexico clays. Sukumaran et al (1999) found that a translational mode of failure will have greater maximum anchor capacity than a rotational mode of failure, applying inclined force will cause greater lateral capacity by reducing caisson rotation, compared with the actual three-dimensional model, a pseudo

three-dimensional model is more time efficient, limiting lateral bearing pressures in offshore piles is smaller than those on deep piles in cohesive soils, installation disturbance of surrounding soils will not reduce the lateral resistance of suction caissons, and finite element analyses can output accurate results and predictions of the capacity of suction caisson, footings and other embedded structures.

Schneider and Senders (2010) presented a summary of considerations for substructure selection and offshore foundation design, and foundations differences between oil & gas industry and offshore wind turbine industry. Schneider and Senders (2010) mentioned several differences occurred in offshore winder turbines: consideration of dynamic behavior, tighter tolerances applied on rotation, monopile deformed as a rigid body but not a flexible body, and the low cost of failure.

Aubeny and Murff (2005) gave an overview of estimating ultimate load capacity of suction caissons by the plastic limit analyses and presented some examples of plastic limit solutions of suction caisson capacity. Aubeny and Murff (2005) mentioned that plastic limit solution is a very good tool when assessing the effects of site and design parameters about caissons capacity, such as load inclination angle, force attachment depth, soil strength profile, surface roughness. Aubeny and Murff (2005) found that the depth of the cable attachment had the greatest influence, the normalized capacity F/Fmax was independent with the caisson geometry ratio Lf/D, and the tip resistance had very small effect on the normalized capacity F/Fmax.

Gerolymos and Gazetas (2006) provided a winkler model utilizing four types of generalized springs to simulate rigid caissons response in a homogeneous elastic soil. In

this model, as mentioned in Gerolymos and Gazetas (2006), spring used the elastic theory of rigid embedded foundations, and simulated how stress distributed along square , rectangular and circular caissons. Gerolymos and Gazetas (2006) compared spring model with the 3D model and did some parametric study of the rectangular caisson loaded by a lateral dynamic force at top.

Zhang, (2016) has developed a 3D finite element by using springs to model surrounding soils and found that the elastic behavior of flexible caissons is very different from that of rigid caissons, ultimate capacity is not influenced by elastic deformations, loading point has a maximum bending stress. Also, Zhang (2016) confirmed that the spring model is very time efficient compare with traditional continuum finite element model.

Luke et al (2005) conducted nine axial pullout tests which were to install a 4 in diameter caisson in a 43 in thick normally consolidated soils. Luke et al (2005) found that dead weight installation had a higher side resistance than that of suction installation, side resistance in a drained condition was the same with that in a undrained condition, sealing caisson had an extremely greater axial capacity, and the reasonable resistance factor was around 0.7 and reasonable end bearing capacity was between 13 and 21.

Ahn et al (2014) provided a finite element method to estimate the holding capacity of the suction caisson without consideration cracks. Ahn et al (2014) found that the normalized shape of the failure envelope was not affected by linear soil profile and affected by the aspect ratio and the depth of optimal loading attachment point was affected by the profile of soil shear strength profile and independent to the dimensions of caissons.

3. CALIBRATION FACTOR

One of key concerns of finite element simulation is choosing a suitable element type. Different element types have different applications. In this research, the main purpose is to simulate the effects of the elastic behavior of caissons on capacity. The elastic deformations of caissons are caused by the contact between caissons and surrounding soils. In order to simulate this contact problem accurately, continuum type elements (C3D8I) are used for suction caissons in this model. However, this type element will make materials stiffer when simulating flexural deformation, which, in this case, is the elastic deformations of caissons. If model cannot simulate caissons' elastic deformation accurately, this research will not achieve its main purpose. Therefore, it becomes very necessary to solve this problem by applying a calibration factor on the elastic modulus of caissons. In order to achieve this goal, a 3D slender circular beam is simulated by ABAQUS. And the result from simulations is compared with that from analytical solution.

3.1 Analytical solution of a slender circular beam

Housner and Vreeland (1965) presented a theoretical solution of the bending of slender circular beams. As shown in Figure 3.1 (After Housner and Vreeland, 1965), there are two diametrically opposed forces P applied on the circular beam. By using the principal of the virtual work, the relative displacement of two forces P shown in Figure 3.1 is given by:

$$u = -0.149\frac{Pr^3}{EI}$$

Where,

u=displacement

p=loading force

r=radius

E=elastic modulus

I=moment of inertia

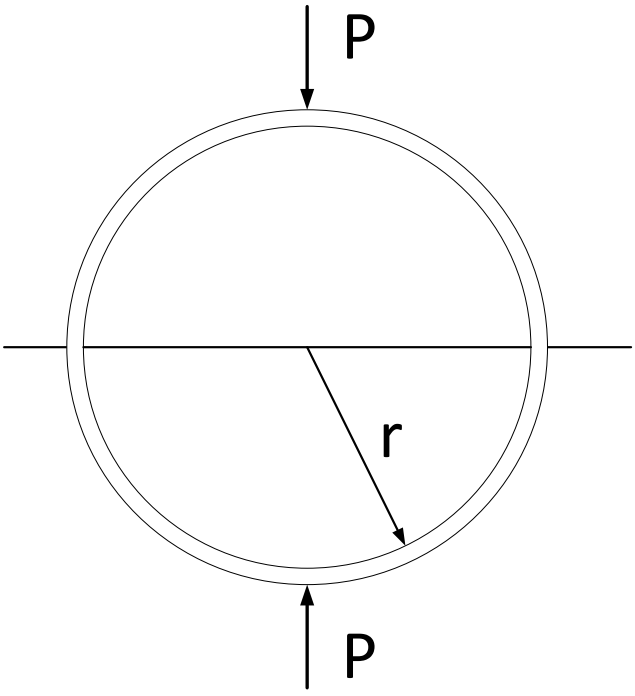

Figure 3.1 Bending of a slender circular beam (After Housner and Vreeland, 1965)

3.2 Simulations of a slender circular beam

The slender circular beam is simulated in this part. Then, the simulation results are compared with the theoretical results mentioned in 3.1 to find out the calibration factors.

3.2.1 Description of model

The slender circular beam is considered as one slice of caissons. Therefore, its mesh, element type and material are the same with these of caissons in the 3-D model. The continuum element C3D8I is used, which is an 8-node brick. This element type is a first-order type element and improved by incompatible modes to enhance their bending behavior. Usually, the conventional element type C3D8 has a “locking” behavior when subjected to bending. This behavior will make element stiffer, reducing bending deformation. The incompatible mode applied in C3D8I can solve this problem by adding internal freedom into elements. This advantage makes it better to for this case. The angular number of elements are 48. The height of an element is 1m. The diameter of circular beam is 5m. As shown in Table 3.1, different thicknesses are applied according to different D/t ratio. The isotropic elastic model is used for material and the properties are assumed as follows: elastic modulus, E = 200000000 kpa, Poisson’s ratio, v = 0.3. As shown in Figure 3.2, the length of model in z direction is used 25m to minimize the effect of accumulated stress in z direction.

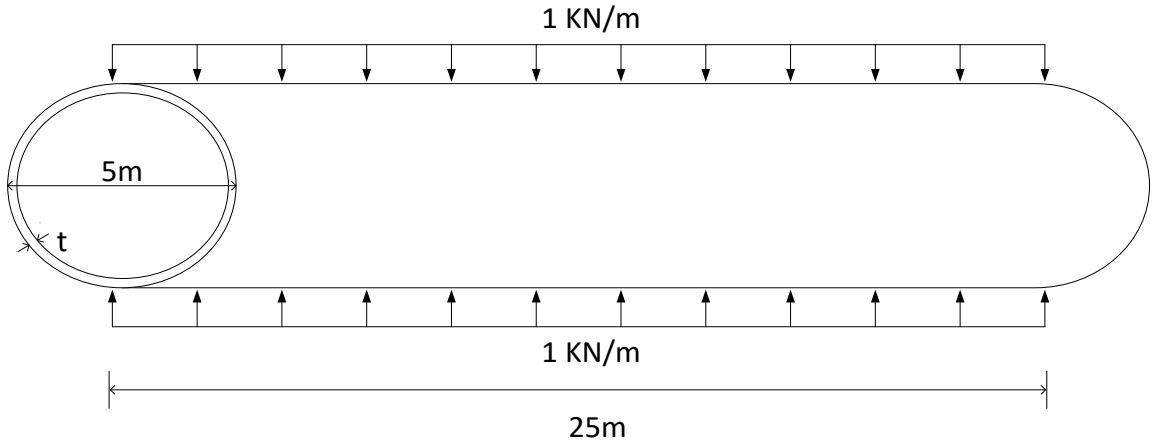

Figure 3.2 Geometry of model

Table 3.1. Thicknesses used in model

D/t (m)	**10**	**20**	**40**	**80**	**160**
t (m)	0.5	0.25	0.125	0.0625	0.03125

The distributed force 1KN/m is applied on the top and the bottom of the circular beam. The relative displacement of the top and bottom at the mid of the length will be measured.

3.3 Results of simulation

The simulation result of thickness 0.0625m is shown in Figure 3.3. As we can see from Figure 3.3, the stress is higher at the side because of the effect of 3D. In order to minimize this negative effect, the relative displacement between top and bottom is selected

at the mid of the length. The displacement from simulations is compared with the result from analytical solution (Table 3.2).

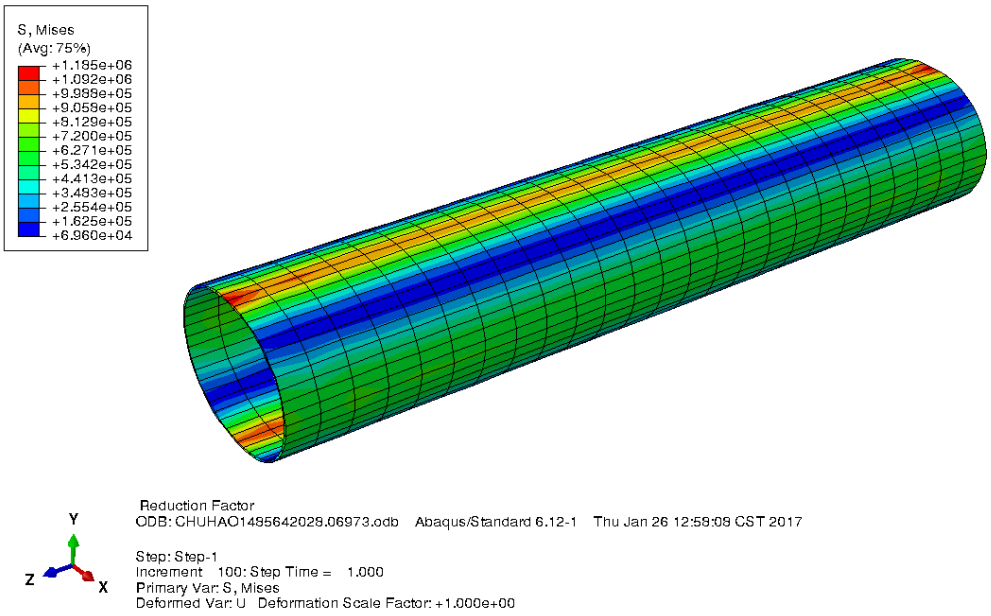

Figure 3.3 Stress distribution of a circular beam

Table 3.2 Calibration factor calculation

P (KN)	δ_{abaqus} (m)	E (KPa)	t (m)	I (m^4)	r (m)	$\delta_{Analytical}$ (m)	Calibration factor
1000	0.505	2E+08	0.0625	2.03E-05	2.5	0.572	0.883

All calibration factors are shown in Table 3.3 and plotted in Figure 3.4. As shown in plotting, the calibration factor is increasing as D/t increasing.

Table 3.3 Calibration factor

D/t	10	20	40	80	160
Calibration factor	0.704	0.768	0.834	0.883	0.901

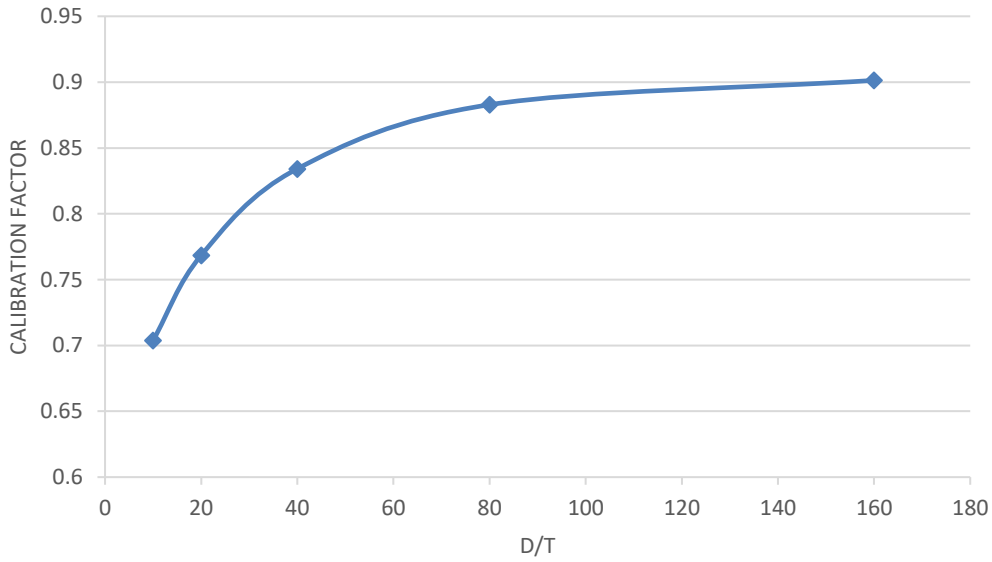

Figure 3.4 Calibration factor vs. D/t

4. FINITE ELEMENT STUDY RESULTS AND DISCUSSIONS

The 3D finite element model used for the analysis was initially developed by Grajales (2017) and has been documented on several papers available in the literature, Murali et al, 2015. FE modeling of caissons are conducted by ABAQUS 6.13 computer program.. The calibration factor discussed in previous section is applied in this finite element analysis. Three different thickness, four different load attachment and two different soil strength are analyzed in this section. In all cases, caissons are loaded in only laterally direction. The results of displacement and capacity are investigated.

4.1 Description of parametric analysis

For all analysis, caissons' diameter is 5m, aspect ratio (L/D) is 3, and soil rigidity index (RI) is 100. Two undrained soil strength are considered in study: linear increasing strength, which is $S_u = 2 + 1.6z$, and constant strength which equals to the average strength of linear profile. Three different thicknesses are included in study, which are 6.250cm, 4.000cm and 3.125cm. Based on discussion in section 3, three corresponding calibration factors are applied to three different thicknesses, which are 0.883 for 6.250cm, 0.898 for 4.000cm, and 0.901 for 3.125cm. Four different locations of load attachment are included in study, which are Li/L=0, Li/L=1/3, Li/L=1/2, and Li/L=2/3 (Li is the distance from the top of caisson to the load attachment point, L is the total length of caissons). All forces are loaded only in laterally direction. According to the parameters shown in above, the matrix of parametric study is summarized in the Table 4.1.

Table 4.1 Parametric analysis

RI	L/D	Soil Strength	D/t	t (cm)	Li/L
100	3	Uniform	80	6.250	0
					1/3
					1/2
					2/3
			125	4.000	0
					1/3
					1/2
					2/3
			160	3.125	0
					1/3
					1/2
					2/3
		$S_u = 2 + 1.6z$	80	6.250	0
					1/3
					1/2
					2/3
			125	4.000	0
					1/3
					1/2
					2/3
			160	3.125	0
					1/3
					1/2
					2/3

4.2 Description of model

The diameter and length of caissons are 5m and 15m. Total length of mesh is three times of caisson's length, which is 45m. The details of model is shown in below.

Element C3D8 is selected to simulate soil. C3D8 is 3D continuum element composed by 8 nodes. However, this element type is fully integrated in ABAQUS, which means it will have "locking behavior". This "locking behavior" will make elements stiffer when subjected to bending deformation. Therefore, C3D8I is selected for caissons. C3D8I is a 3D continuum element composed by 8 nodes and is improved by incompatible modes to enhance its accurate when simulate bending behavior.

There are two materials in this model. One is soil, whose material model is elastic perfectly plastic model, with Mohr Coulomb as yield criterion. The undrained shear strength equals to 14 kpa in uniform soil strength profile and 2+1.6z kpa in linear soil strength profile. Properties of soil's material model is presented in Table 4.2. Another material is caisson. For this model, caissons are considered as steel. Therefore, linear elastic material model is used. The elastic modulus equals to steel's elastic modulus, 2E8 kpa, multiplying calibration factor discussed in section 3. Properties of caissons' material is presented in Table 4.3. Model is loaded laterally by displacement control. The total loaded displacement is 2.5m.

Table 4.2 Properties for soil material model

Elastic Modulus (kpa)	Poisson's Ratio	Friction Angle	Dilation Angle	Cohesion yield stress (kpa)
4200	0.49	0°	0°	14

Table 4.3 Properties for caisson's material model

Thickness (m)	Calibration Factor	Steel's Elastic Modulus (kpa)	Caisson's Elastic Modulus (kpa)	Poisson's Ratio
0.0625	0.883	2E8	1.766E8	0.3
0.04	0.898	2E8	1.796E8	0.3
0.03125	0.901	2E8	1.802E8	0.3

4.3 Analysis results

Three parameters have been analyzed, which are location of load attachment, thickness of caissons, and soil strength profile. The results from simulation are shown in below. The reaction forces in the figures are considered as capacities corresponding to different displacements.

4.3.1 Effect of location of load attachment

The results of reaction force versus displacement for 6.25cm thick caissons and uniform soil strength profile is shown in Figure 4.1. The results of reaction force versus displacement for 4.00cm thick caissons and uniform soil strength profile is shown in Figure 4.2. The results of reaction force versus displacement for 3.125cm thick caissons and uniform soil strength profile is shown in Figure 4.3. The results of reaction force

versus displacement for 6.25cm thick caissons and linear soil strength profile is shown in Figure 4.4. The results of reaction force versus displacement for 4.00cm thick caissons and linear soil strength profile is shown in Figure 4.5. The results of reaction force versus displacement for 3.125cm thick caissons and linear soil strength profile is shown in Figure 4.6.

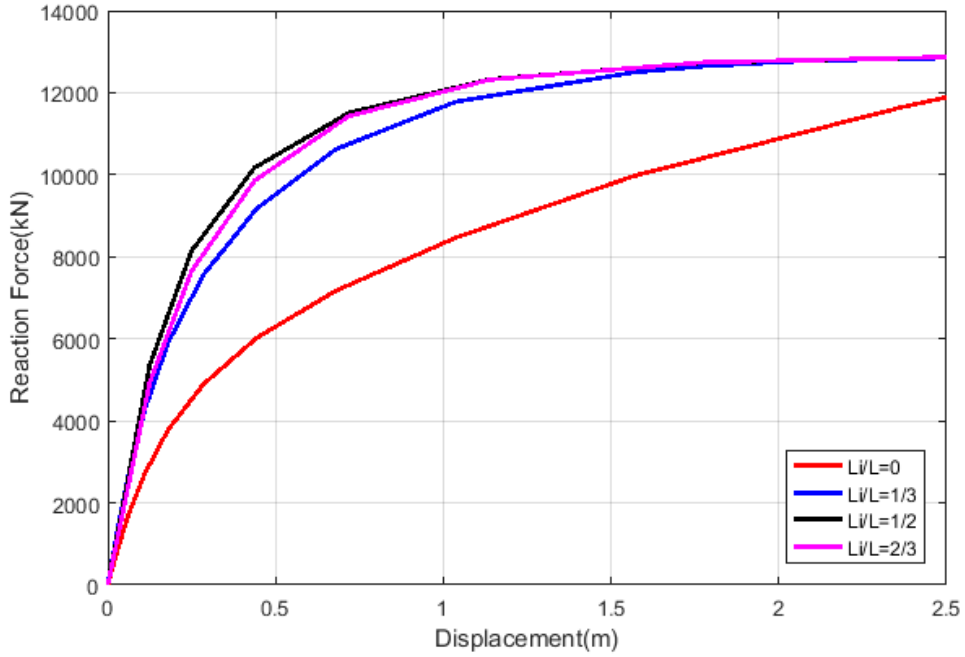

Figure 4.1 Loading-displacement curve of 6.25cm thick caissons and uniform soil strength

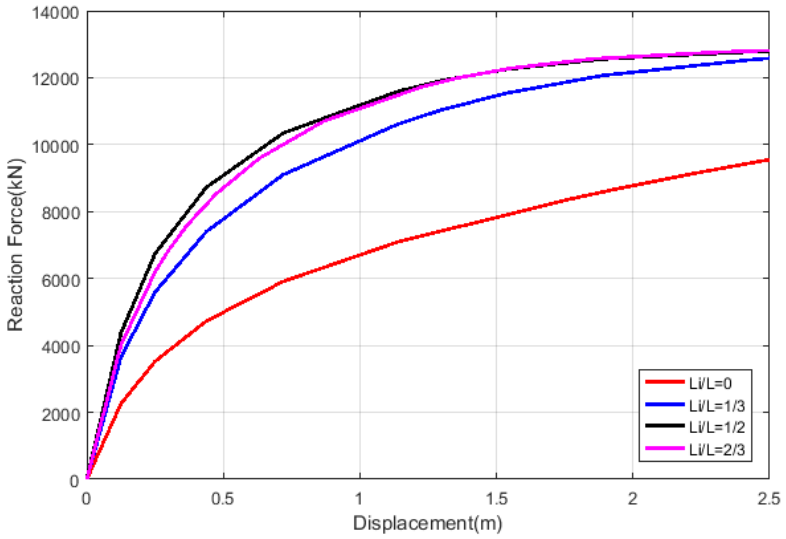

Figure 4.2 Loading-displacement curve of 4.00cm thick caissons and uniform soil strength

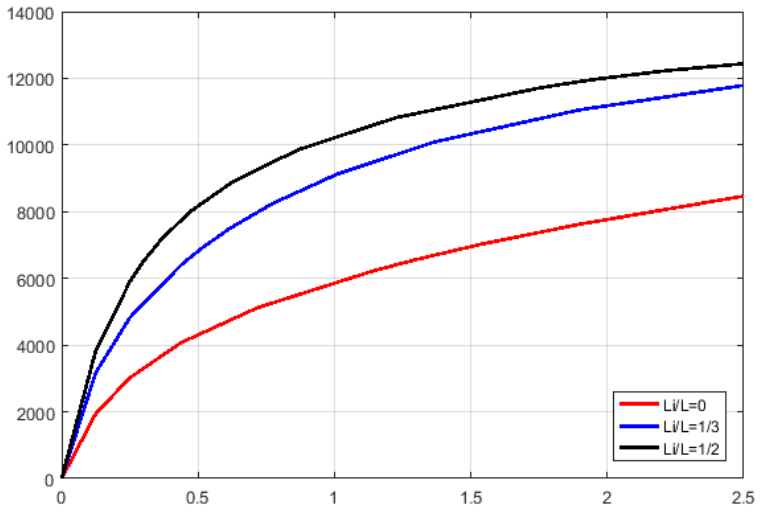

Figure 4.3 Loading-displacement curve of 3.125cm thick caissons and uniform soil strength

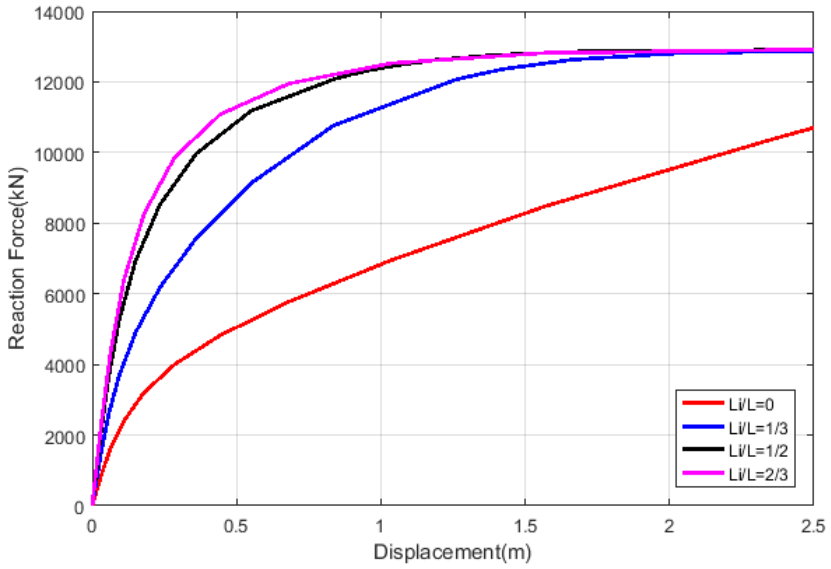

Figure 4.4 Loading-displacement curve of 6.25cm thick caissons and linear soil strength

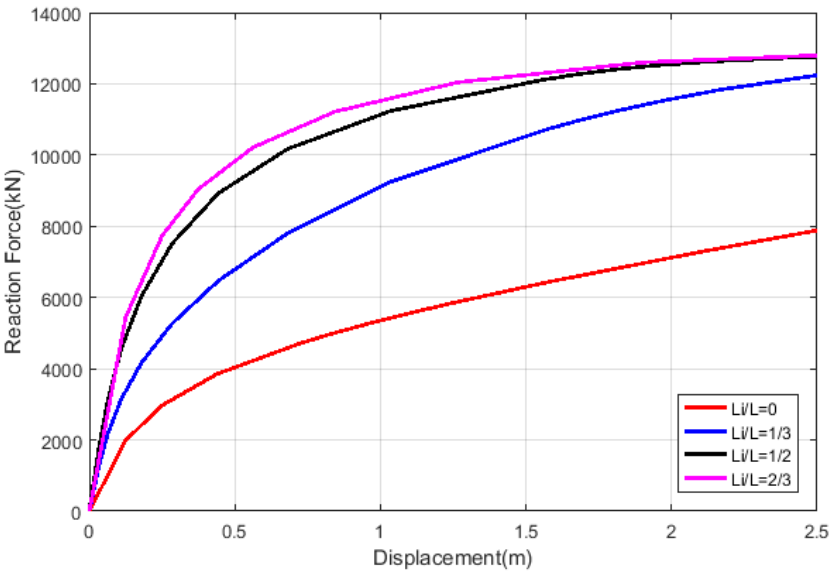

Figure 4.5 Loading-displacement curve of 4.00cm thick caissons and linear soil strength

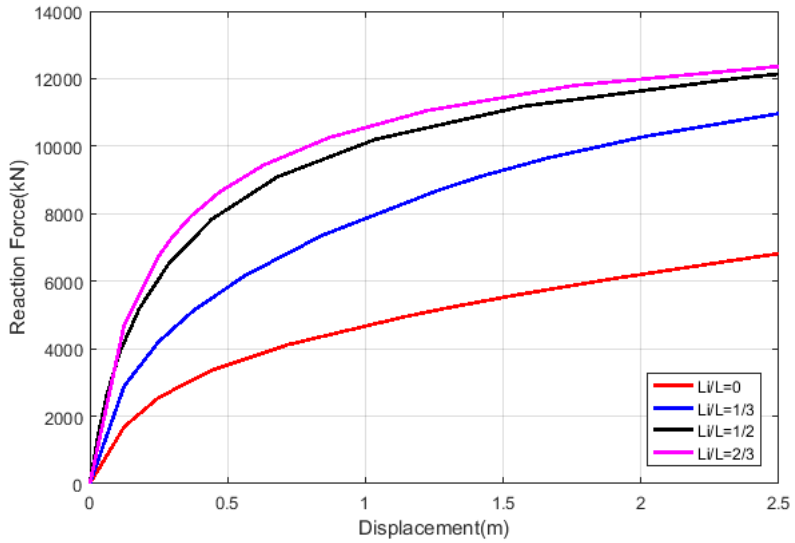

Figure 4.6 Loading-displacement curve of 3.125cm thick caissons and linear soil strength

According to the above results, for uniform soil strength profile, the optimal load attachment location is Li/L=1/2. However, for linear soil strength profile, the optimal load attachment location is Li/L=2/3. For uniform soil strength profile, no matter what thickness caisson has, the capacity of caissons decreases while attachment location moving from Li/L=1/2 to the top, and increases while attachment location moving from Li/L=2/3 to Li/L=1/2. However, for linear soil strength profile, no matter what thickness caisson has, the capacity of caissons decreases while attachment point moving toward the top.

4.3.2 Effect of thickness

The results of reaction force versus displacement for Li/L=1/2 and uniform soil strength profile is shown in Figure 4.7. The results of reaction force versus displacement

for Li/L=1/3 and uniform soil strength profile is shown in Figure 4.8. The results of reaction force versus displacement for Li/L=2/3 and linear soil strength profile is shown in Figure 4.9. The results of reaction force versus displacement for Li/L=1/2 and linear soil strength profile is shown in Figure 4.10. The results of reaction force versus displacement for Li/L=1/3 and linear soil strength profile is shown in Figure 4.11.

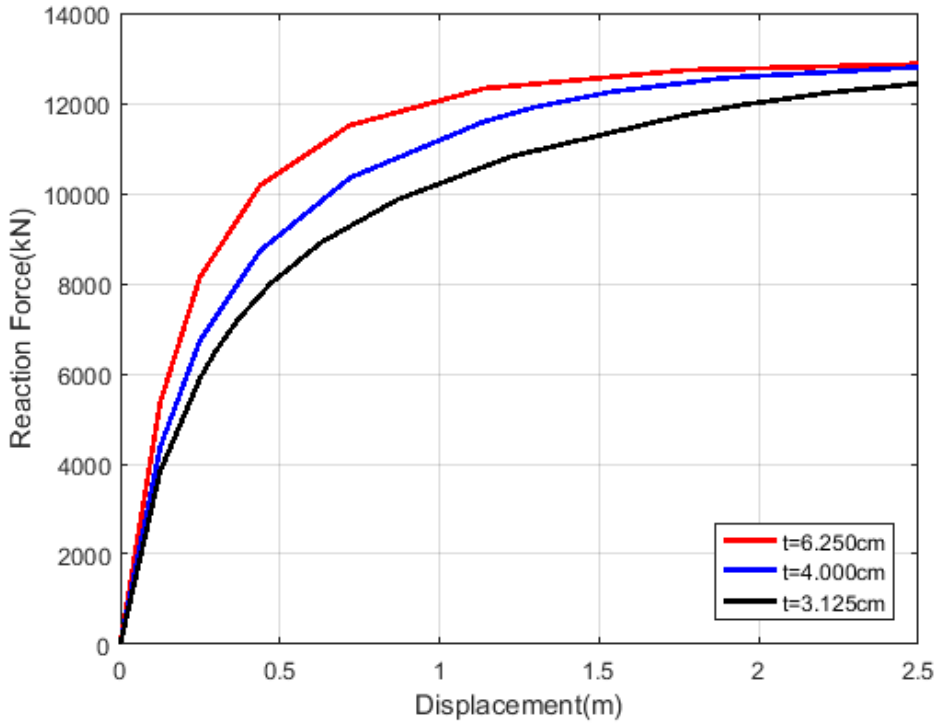

Figure 4.7 Loading-displacement curve of Li/L=1/2 and uniform soil strength

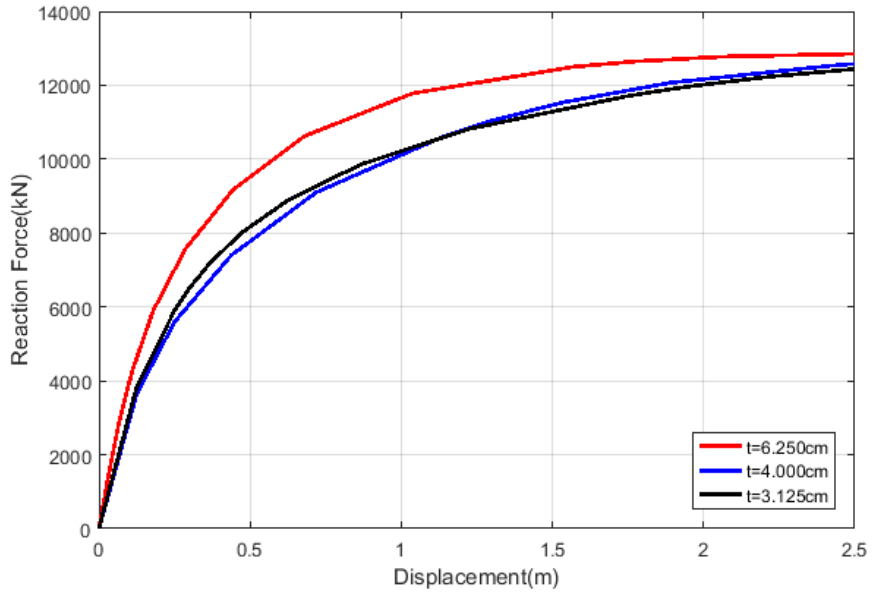

Figure 4.8 Loading-displacement curve of Li/L=1/3 and uniform soil strength

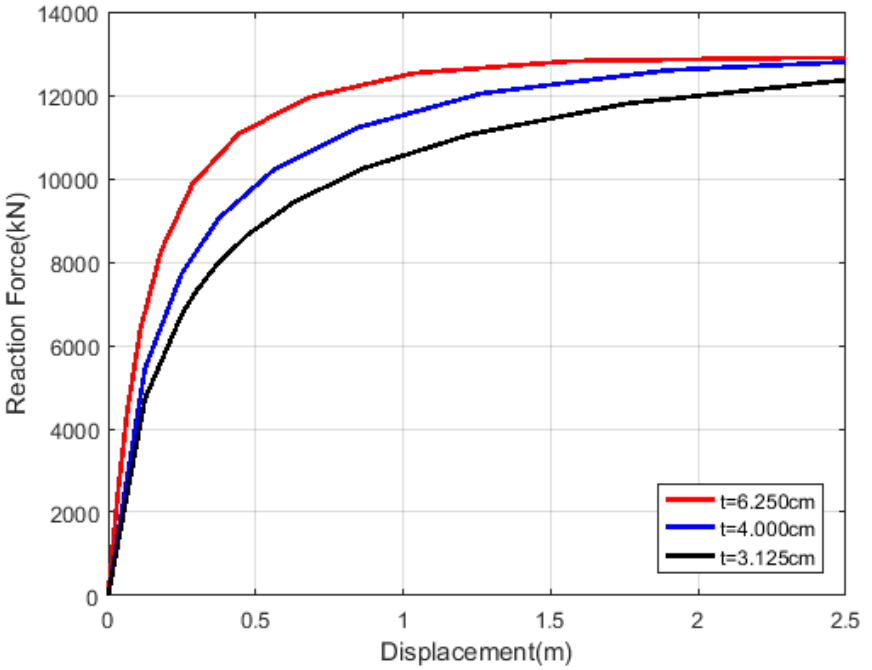

Figure 4.9 Loading-displacement curve of Li/L=2/3 and linear soil strength

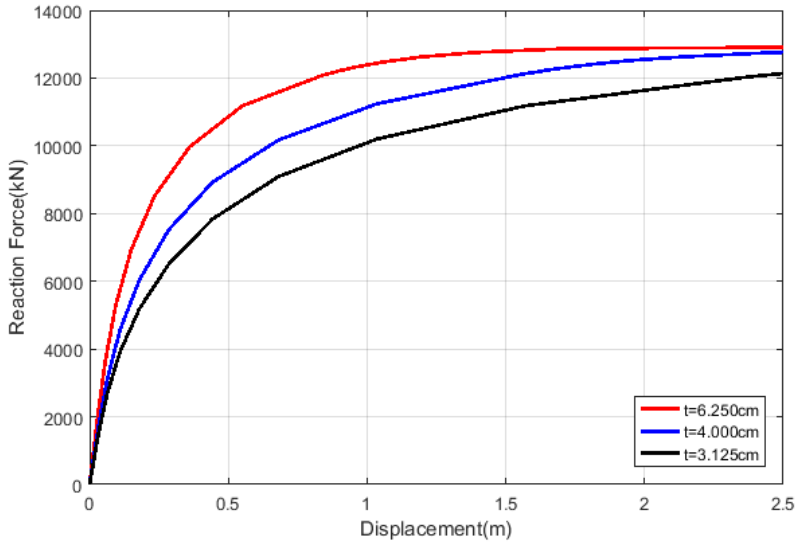

Figure 4.10 Loading-displacement curve of Li/L=1/2 and linear soil strength

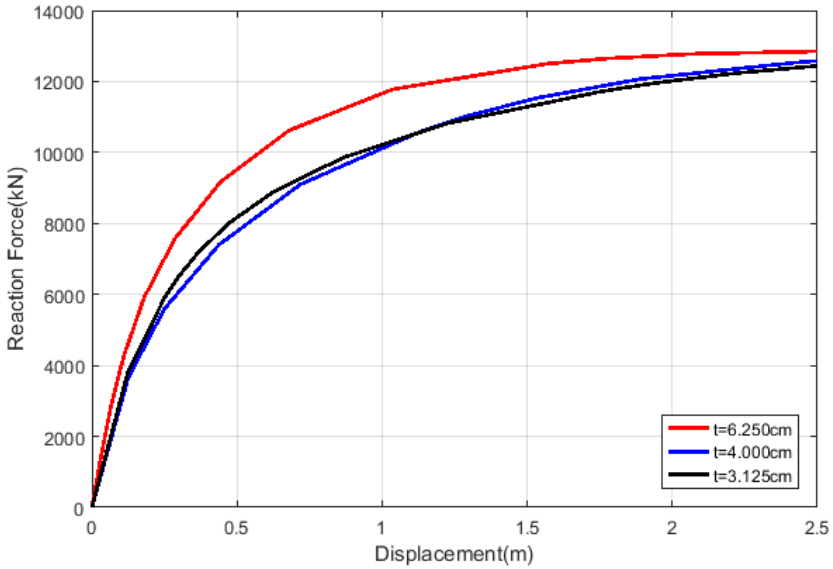

Figure 4.11 Loading-displacement curve of Li/L=1/3 and linear soil strength

According to above results, 6.25cm thick caisson has the greatest capacity. The reason may be that 6.25 cm is the largest thickness in above result. For load attachment located at Li/L=1/2, no matter what soil strength profile mode uses, the capacity increases with thickness increases. However, for load attachment located at Li/L=1/3, the changing tendency of capacity is different with previous results. As we can see from Figure 3.8 and Figure 3.11, although 6.25cm thick caisson still has the largest capacity, the capacity of 3.125cm thick caissons is larger than that of 4.00cm thick caissons when displacement is less than 1.25m, and the capacity of 3.125cm thick caissons is smaller than that of 4.00cm thick caissons when displacement is more than 1.25m. The load attachment of caisson will influence the changing tendency of capacity for different thicknesses.

4.3.3 Effect of soil strength profile

The results of reaction force versus displacement for Li/L=1/3 and 6.25cm thickness is shown in Figure 4.12. The results of reaction force versus displacement for Li/L=1/2 and 6.25cm thickness is shown in Figure 4.13. The results of reaction force versus displacement for Li/L=2/3 and 6.25cm thickness is shown in Figure 4.14. The results of reaction force versus displacement for Li/L=1/3 and 4.00cm thickness is shown in Figure 4.15. The results of reaction force versus displacement for Li/L=1/2 and 4.00cm thickness is shown in Figure 4.16. The results of reaction force versus displacement for Li/L=2/3 and 4.00cm thickness is shown in Figure 4.17.

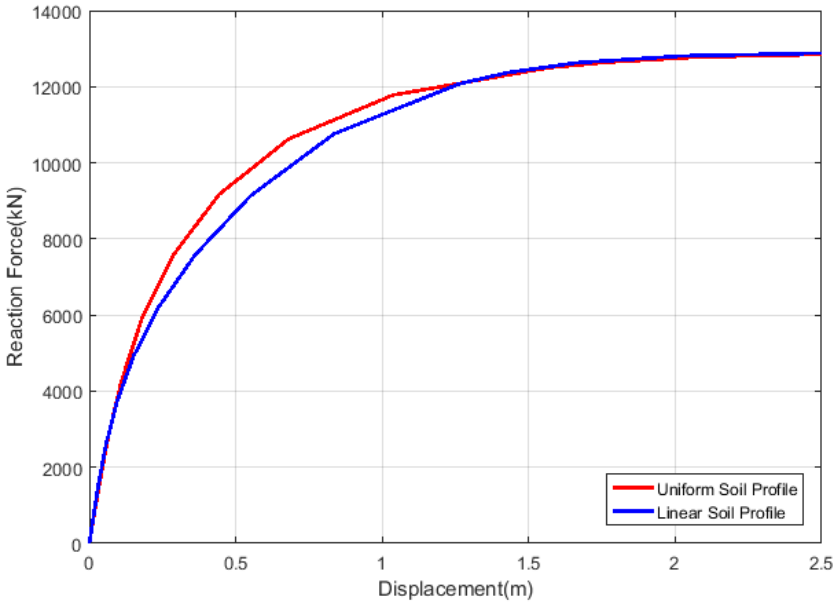

Figure 4.12 Loading-displacement curve of Li/L=1/3 and 6.25cm thickness

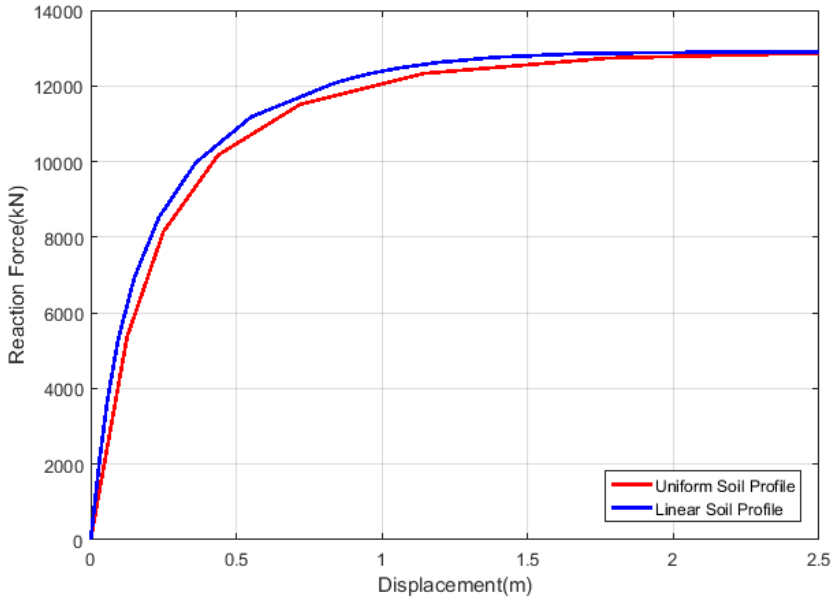

Figure 4.13 Loading-displacement curve of Li/L=1/2 and 6.25cm thickness

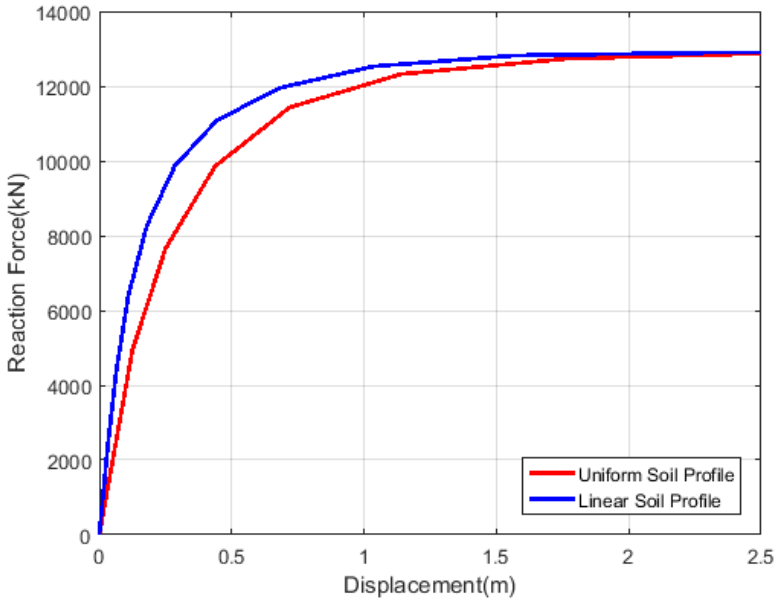

Figure 4.14 Loading-displacement curve of Li/L=2/3 and 6.25cm thickness

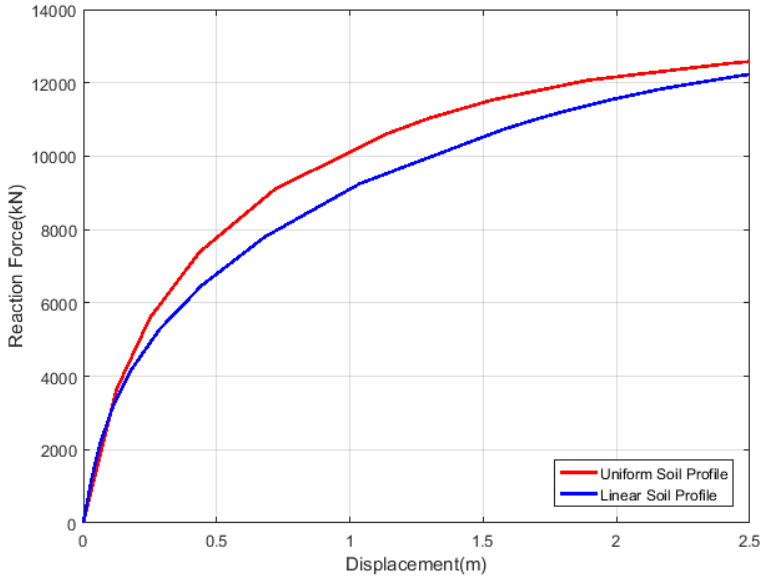

Figure 4.15 Loading-displacement curve of Li/L=1/3 and 4.00cm thickness

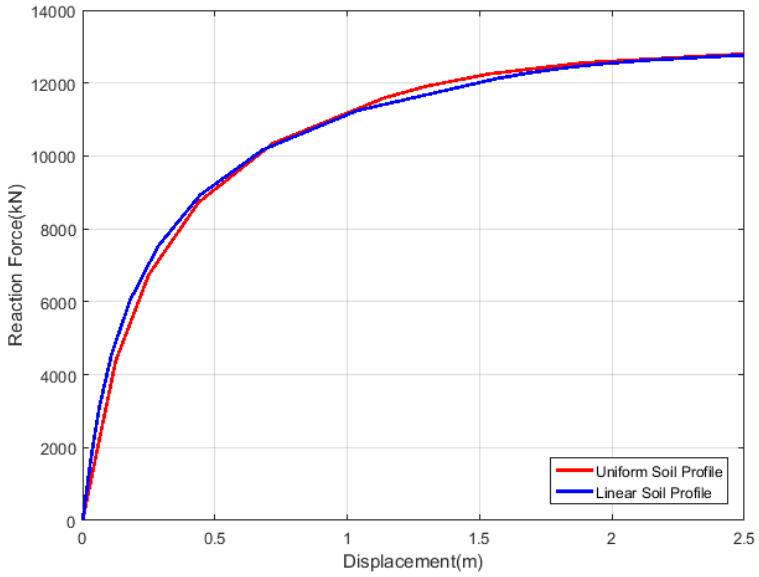

Figure 4.16 Loading-displacement curve of Li/L=1/2 and 4.00cm thickness

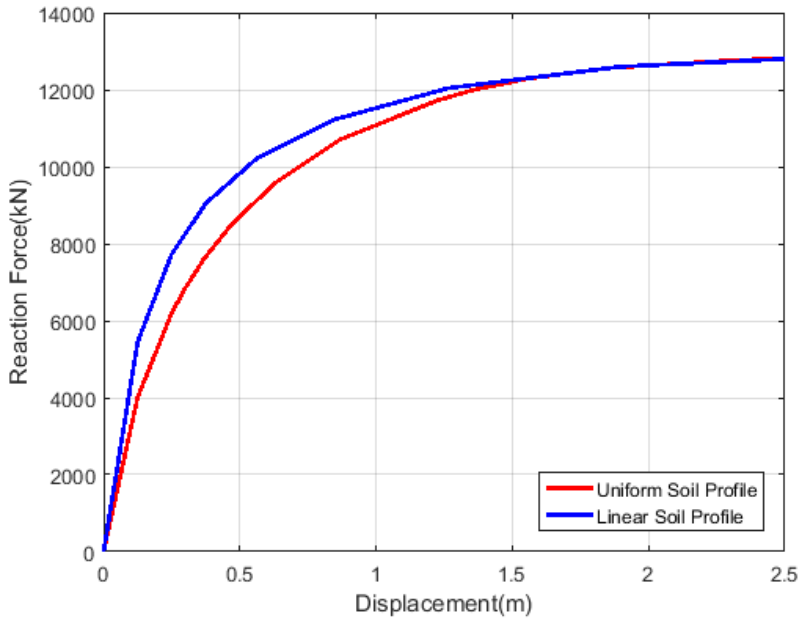

Figure 4.17 Loading-displacement curve of Li/L=2/3 and 4.00cm thickness

The above results indicate that, for 6.25cm thickness, when load attachment is located at Li/L=1/3, the capacity of using uniform soil strength profile is greater than that of using linear soil strength profile, however, when load attachment is located at Li/L=1/2 and Li/L=2/3, the capacity of using uniform soil strength profile is less than that of using linear soil strength profile. For 4.00cm thickness, when load attachment is located at Li/L=1/3, the capacity of using uniform soil strength profile is greater than that of using linear soil strength profile, and when load attachment is located at Li/L=2/3, the capacity of using uniform soil strength profile is less than that of using linear soil strength profile. However, when load attachment is located at Li/L=1/2, the capacity of using uniform soil strength profile is smaller than that of using linear soil strength profile at the small displacement, and the capacity of using uniform soil strength profile is greater than that of using linear soil strength profile at the large displacement.

4.3.4 Stress contour

The stress contours are plotted to investigate the structural responses. For this analysis, average Mises stress is investigated. The contours for load attachment at Li/L=1/2 with different thickness and different soil profile are shown from Figure 4.18 to Figure 4.23. Since the deformation of caissons is too small to tell, a deformation scale factor 2 is applied to all contours.

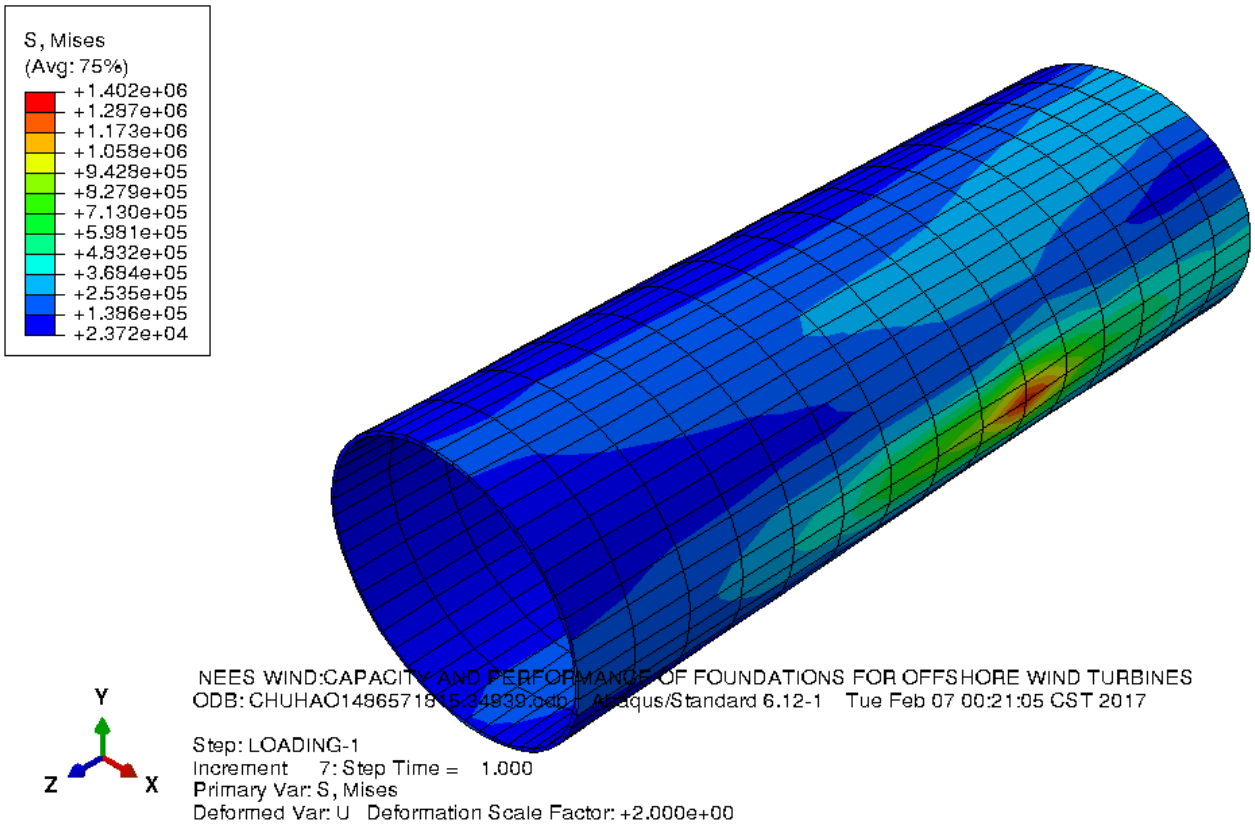

Figure 4.18 Stress contour for Li/L=1/2, 6.25cm thick and uniform soil strength profile

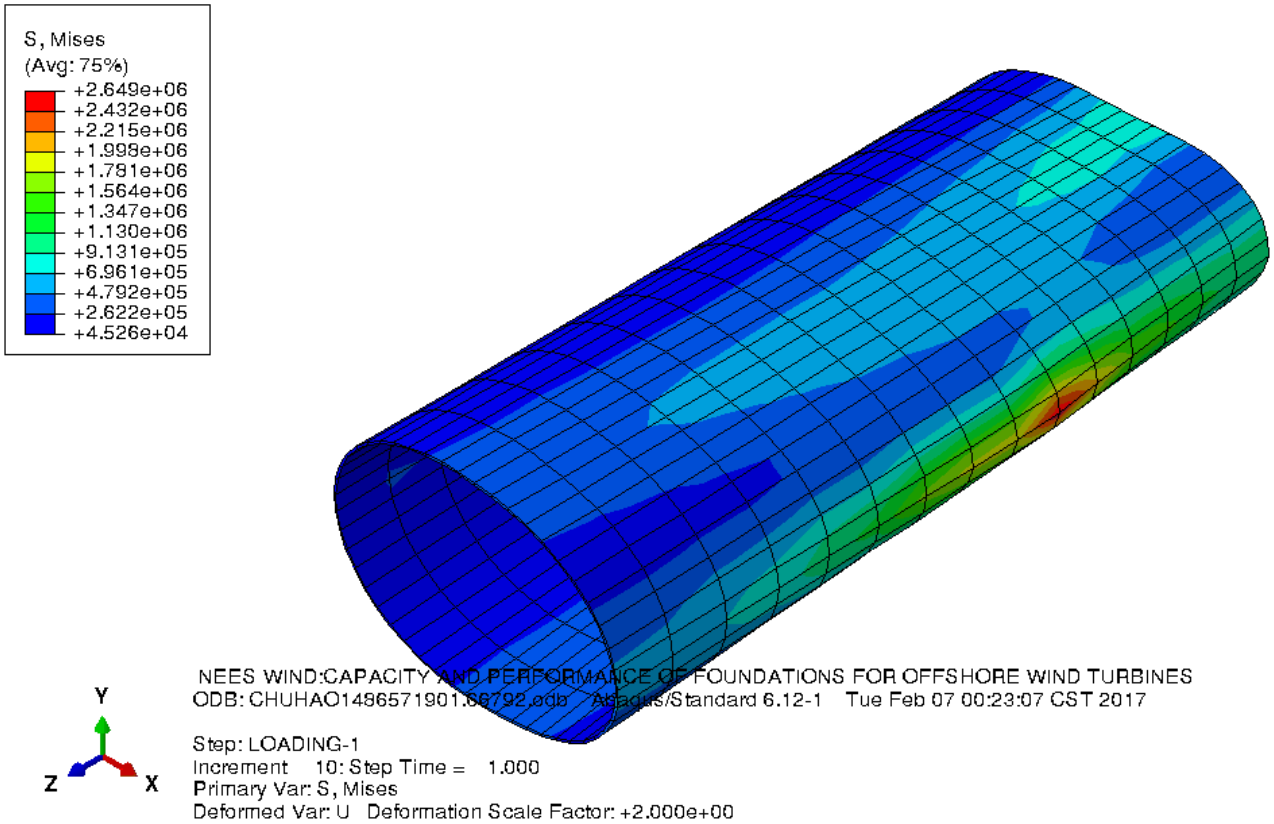

Figure 4.19 Stress contour for Li/L=1/2, 4.00cm thick and uniform soil strength profile

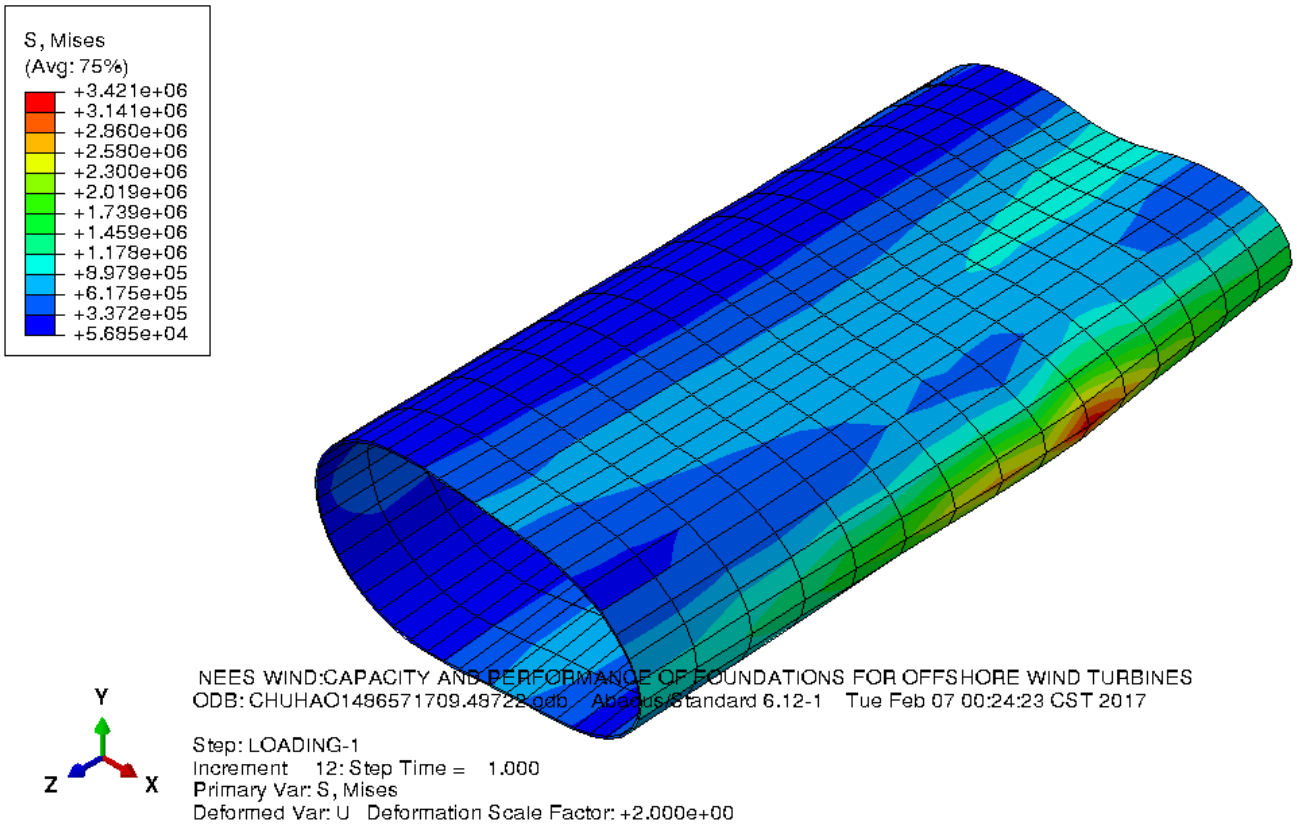

Figure 4.20 Stress contour for Li/L=1/2, 3.125cm thick and uniform soil strength profile

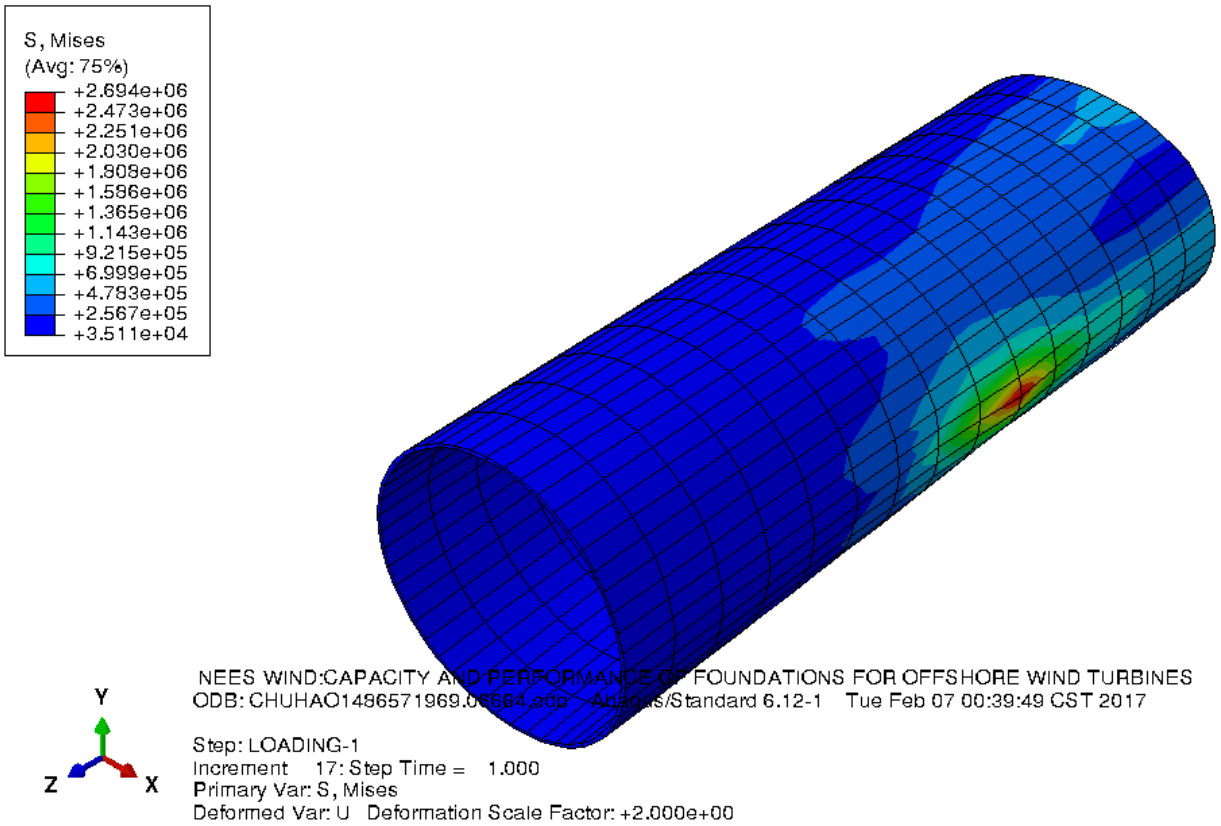

Figure 4.21 Stress contour for Li/L=1/2, 6.25cm thick and linear soil strength profile

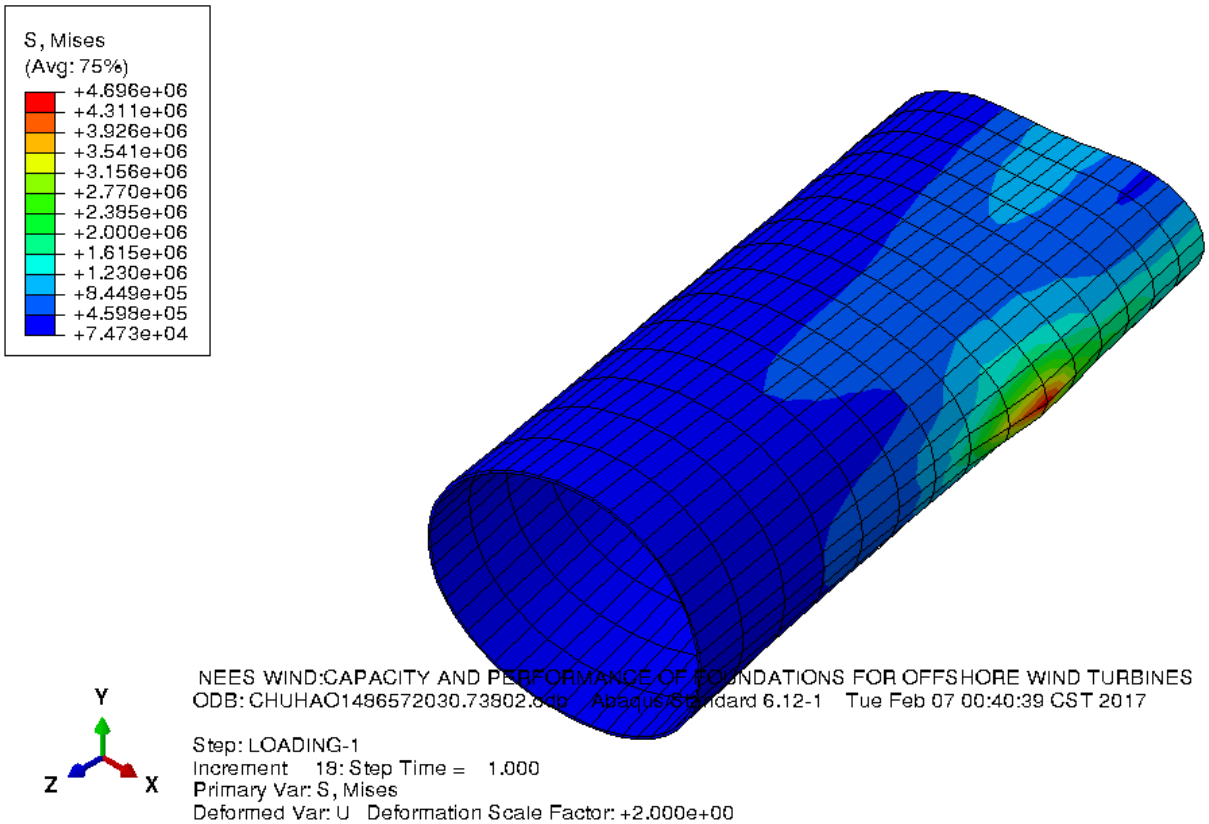

Figure 4.22 Stress contour for Li/L=1/2, 4.00cm thick and linear soil strength profile

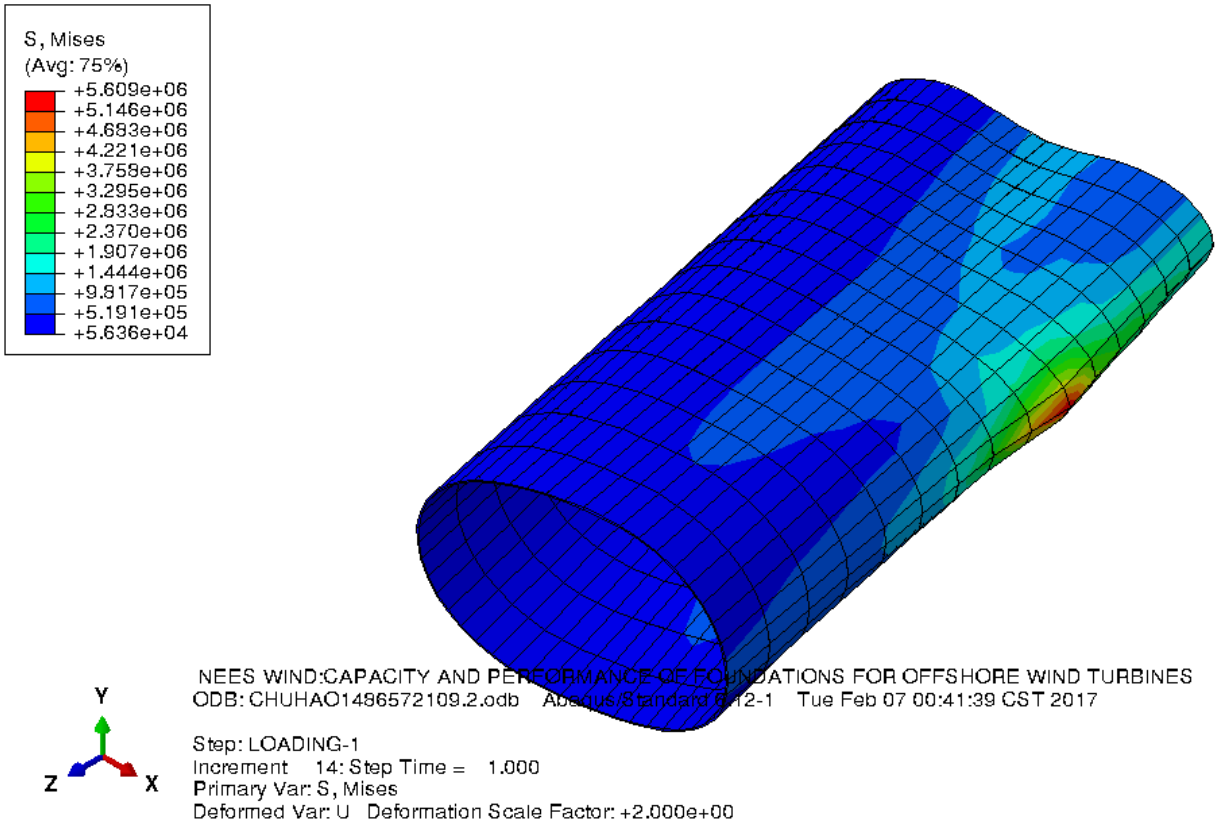

Figure 4.23 Stress contour for Li/L=1/2, 3.125cm thick and linear soil strength profile

The results show that the max stress always occurs at the load attachment point. For both soil strength profiles, the max stress is larger in thinner caisson. This conclusion means increasing thickness of caissons will help reduce the max stress. And the thinner the caisson is, the greater the deformation is.

Also, there are differences when using different soil strength profiles. The increase of stress of using uniform soils strength profile is less than that of using linear soil strength profile. And when using uniform profile, the deformation of caissons is uniform along length. However, when using linear profile, there is a heave at load attachment. This means soil strength profile will influence the deformation a lot. Therefore, it is important to choose a reasonable soil strength profile when simulating an actual case.

5. DEVELOPMENT OF SPRING PROPERTIES

The main purpose of this section is to generate springs properties which can simulate the soil contact force around caissons in 3D continuum model and compare these spring properties with the results in Zhang, 2016.

5.1 Method of generating spring properties

The model selected to generate spring properties is using uniform soil profile, 4cm thick, RI=100, $E_{caisson}$=2E8 kpa and load attachment at Li/L=1/2. The NFORC1, NFORC2, U1 and U2 are outputted for all nodes on the caisson. The NFORC1 and NFORC2 are chosen from element nodal variables. As shown in Figure 5.1, the NFORC1, NFORC2, U1, and U2 are translated from x and y directions into tangential and radial directions by following equations,

$$F_r = F_x cos\theta + F_y sin\theta$$

$$F_t = F_x sin\theta - F_y cos\theta$$

$$U_r = U_x cos\theta + U_y sin\theta$$

$$U_t = U_x sin\theta - U_y cos\theta$$

All these variables are based on global coordinates. Therefore, the total radial nodal force are calculated by adding the inner radial nodal force to outer radial nodal force. The total tangential nodal force are calculated by adding the inner tangential nodal force to outer tangential nodal force. In order to compare with results in Zhang, 2016, the net radial nodal force and tangential force are divided by nodal area and soil strength, which

are 0.33 and 14. Nodal area is equal to the element area on caisson and calculated by following equation,

$$dA = dL \times dZ$$

Where,

$$dL(length\ of\ element) = \frac{\pi D}{48}$$

$$dZ(height\ of\ element) = \frac{L}{n}$$

D is a diameter of caisson, which equals to 5m. 48 is the number of elements in theta direction. L is the length of caisson, which equals to 15m. n is the number of element in length direction of caisson, which equals to 15.

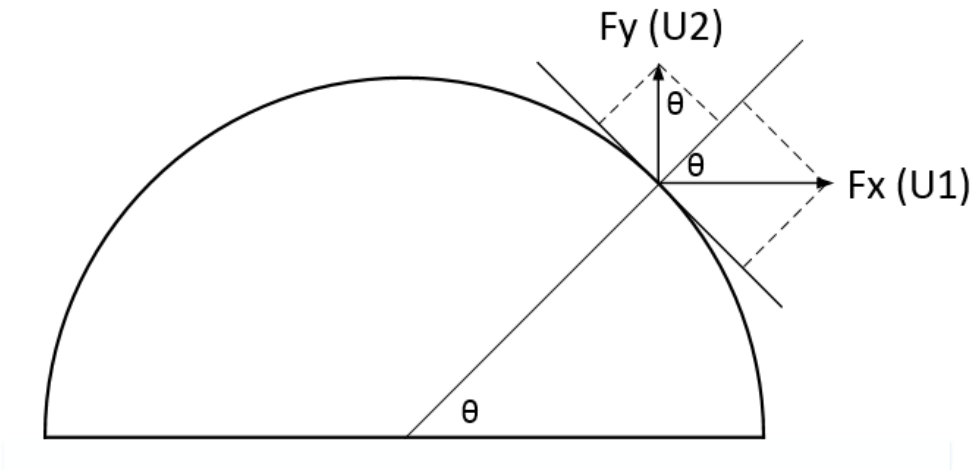

Figure 5.1 Diagram of transferring variables into radial and tangential direction

5.2 Spring loading-displacement curves

The spring loading-displacement curves for 23 angles are plotted for a rigid caisson at 6-meter depth. The radial spring loading-displacement curves are shown in Figure 5.2. The tangential spring loading-displacement curves are shown in Figure 5.3.

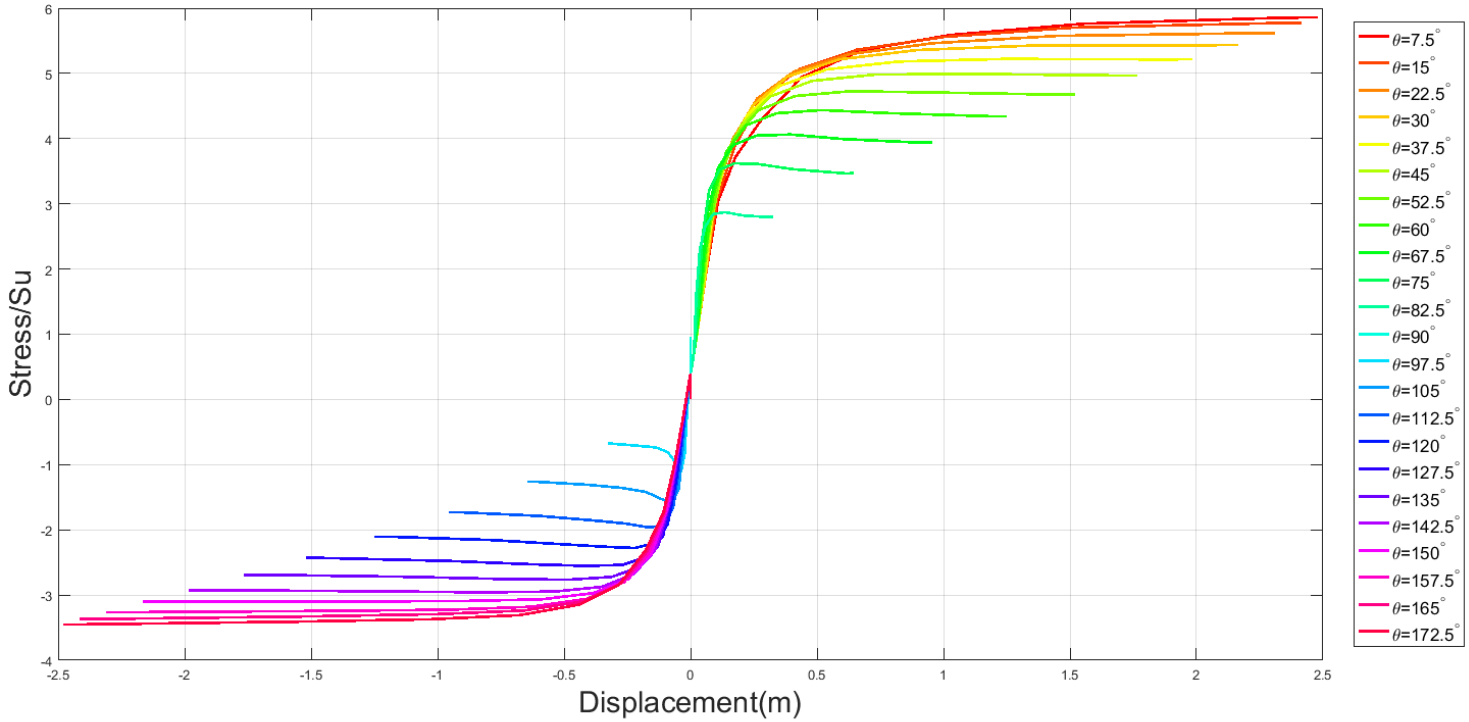

Figure 5.2 Radial loading-displacement curves at 6m depth.

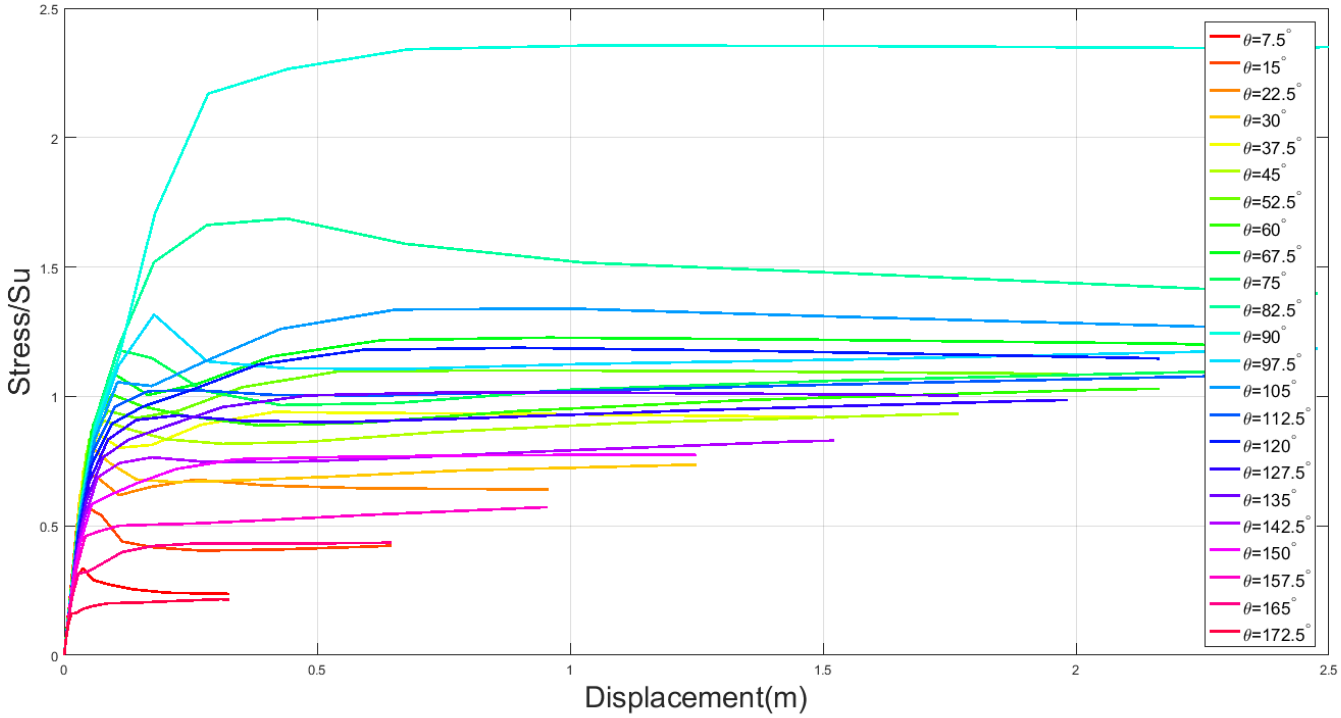

Figure 5.3 Tangential spring loading-displacement curves at 6m depth.

As shown in Figure 5.2, when angles range from 7.5° to 90°, the spring curve's ultimate forces are decreasing with angle increasing. However, when angles range from 90° to 172.5°, the absolute values of spring curve's ultimate forces are decreasing with angle increasing. And the big picture is kind of centrosymmetric. The absolute value of max possitive force is always larger than that of max negative force. So is the displacement. It means that, its "front face", which is from 0° to 90°, is subjected to larger deformation and force than "back face", which is from 90° to 180°.

As shown in Figure 5.3, loading-displacement curves for all angles can divided into three parts. In part 1, 7.5° to 45°, curves' ultimate forces are increasing with angle increasing and curves' max forces are equal to their ultimate forces. In part 2, 52.5° to 82.5°, there is a peak in every curve before reaching ultimate force and this peak occurs at larger displacement when angle increasing. Although these curves have a peak whose value is larger than ultimate, their ultimate forces are constant with changing angles. In part three, 97.5° to 172.5°, there are also a peak in every loading-displacement curve. However, their ultimate forces are decreasing with angle increasing.

Many ultimate normalized stresses in Figure 5.3 are over 1. This phenomenon is not reasonable. The possible reason is that this model does not take slippery into considerations. Therefore, the tangential stress can surpass soil shear strength. More researches are needed in the tangential stresses.

5.3 Comparisons with other spring curves

Zhang, 2016 has exported spring properties from a 2D model and used them in 3D simulations of caissons. The aim of this section is to compare loading-displacement curves from 3D model with these from Zhang, 2016.

In order to minimize z dimensional effect, spring curves at 15m depth are selected for comparisons. The comparison of all radial loading-displacement curves is shown in Figure 5.4.

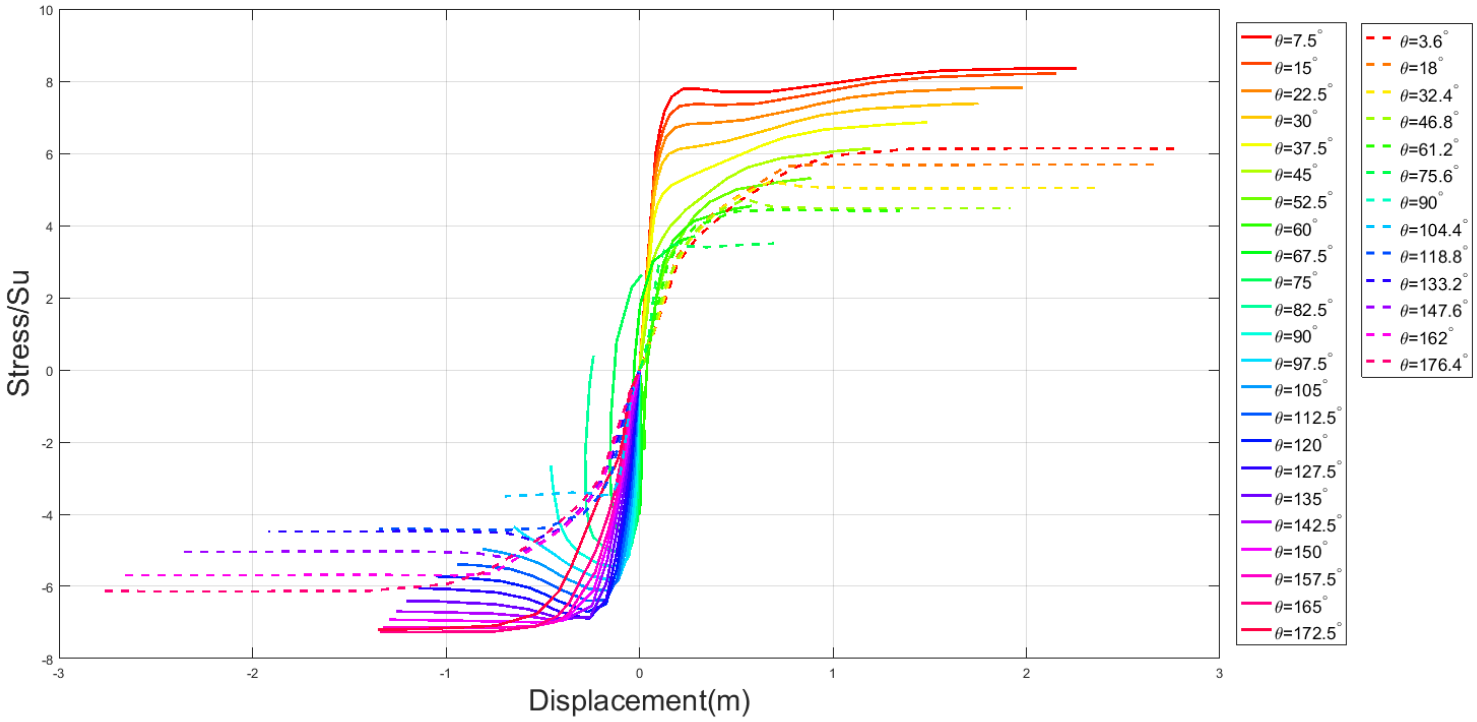

Figure 5.4 Comparison of all radial spring curves from two models.

(Solid line stands for curves from this research, dashed line stands for curves from Zhang, 2016)

According to Figure 5.4, the absolute values of ultimate forces for every spring curves from this research are larger than these from reference. Another difference is that there are some intergradation curves, shown in Figure 5.5, in results from this research. However, there are no such curves in reference.

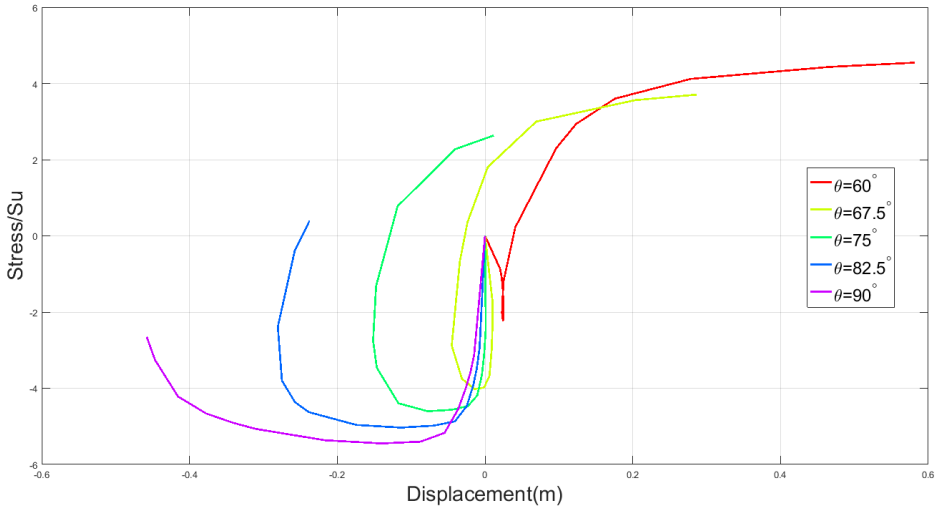

Figure 5.5 Intergradation curves

This difference is possible caused by 3D dimensional effect. In 2D model, used in reference, surrounding soil is easy to flow around the caisson. However, in 3D model, it is more difficult and complicated for soil flowing, causing caisson to deform at the edge of circle, which is 60° to 90°. The intergradation spring curves occur in location marked in Figure 5.6. In order to see the deformation of marked points, the deformation scale is set to 3. It is obvious that there are greater deformations of marked points than these of other points in the same depth. This phenomenon could explain why intergradation curves

occur in these points. Also, it can partly be indicated that 2D model did not catch this phenomenon.

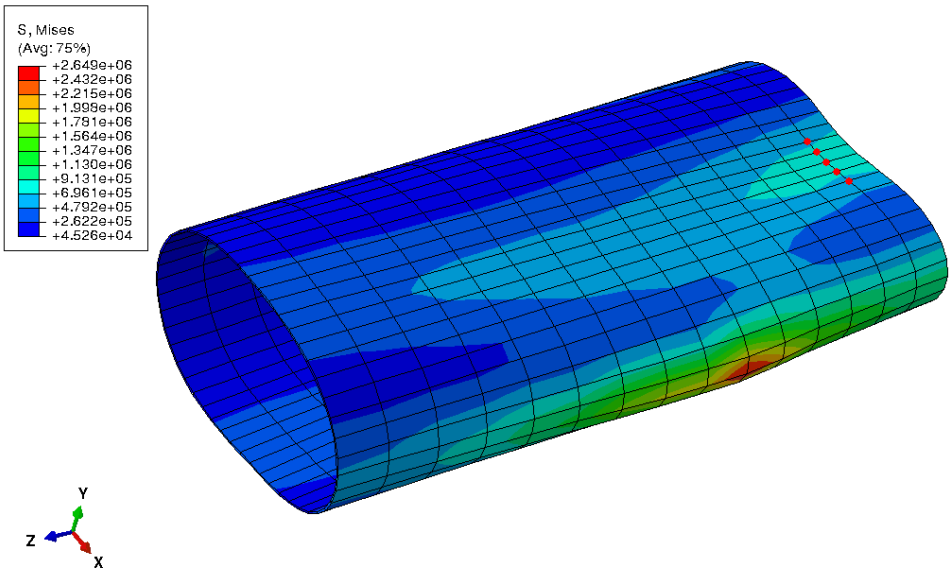

Figure 5.6 Marked points on caisson

As the angles for spring curves from two models are not the same, two angles, 3.6°and 18°, in reference and two nearby angles, 7.5° and 15°, in this research are selected for comparing differences between single curve.

As shown in Figure 5.7, forces for all displacement in this research are always larger than these of reference. The common things between two results is that initially two loading-displacement curves for different angles share the same curve and then reach different ultimate forces.

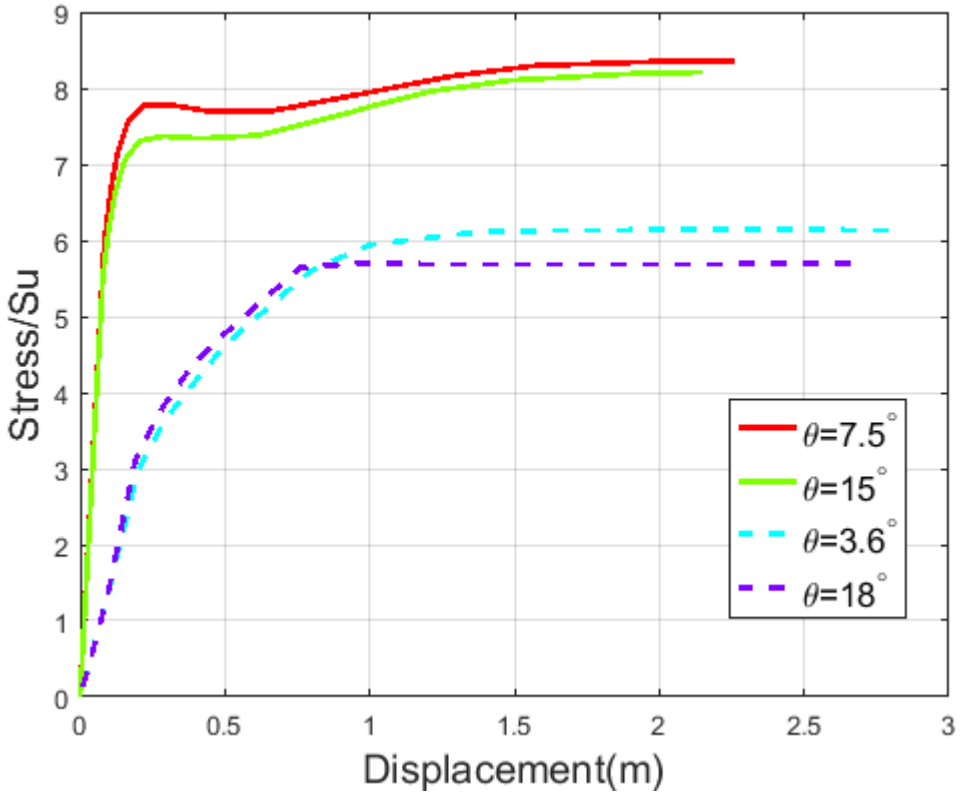

Figure 5.7 Comparison of four loading-displacement curves

(Solid line stands for loading-displacement curve from 3D model. Dash line stand for loading-displacement curve from reference)

6. CONCLUSIONS

The 3D continuum finite element simulation provided a lot of variable results of effect of elastic behavior on the capacity of caisson.

The most important finding in this study is that elastic behavior indeed has a lot effects on caisson's capacity, which means that we cannot consider caissons as rigid body when designing. Especially, when displacement is small, the elastic caisson has smaller capacity than that of rigid caisson. What's more, for elastic caisson, when loading attachment location surpasses Li/L=1/2 and thickness equals to 6.25cm, caisson's capacity will decrease. Also parametric study shows that different soil profiles will also greatly affect capacity, which means it is important to choose suitable soil strength profile when calculating capacity.

The surrounding soil forces and corresponding displacements are transferred into spring loading-displacement curves. From these spring properties, we can know how the caisson structural response is. One of these findings is that the edge of caisson's front face, which is 60° to 90°, has a relative large deformation than other part of caisson. It means that when designing, this edge should be strengthen to deal with large deformation. Also, by comparing loading-displacement curves from this study with the results from 2D model, some differences are noticed, which are possibly caused by z dimensional effects. First difference is that the ultimate forces for every loading-displacement curves in 3D model is always larger than corresponding forces in 2D model (reference). And there are some intergradation curves plotted from 3D model, which are not plotted in results from 2D model.

As the limit of time, this thesis cannot consider all factors that will affect results. Therefore, there are some recommendations for further study.

In section 3, calibration factors are calculated by comparing displacement from 3D simulation and 2D theoretical solution. Firstly, theoretical solution may be not accurate. It is better to compare results with that from experiments. Secondly, the theoretical solution is for 2D problem, which means it may be not accurate for 3D problem. It is better to choose 3D theoretical solution.

In section 5, spring properties are plotted by outputting node force (NFORC) and displacement (U) in ABAQUS. As spring stands for surrounding soils, the force we need is the contact force between soils and caissons. However, node force is the internal force of each node, which includes more than contact force. Therefore, it is better to output contact force by adding contact pairs between soils and caissons.

REFERENCES

Ahn, J., Lee, H., & Kim, Y. T. (2014). Holding capacity of suction caisson anchors embedded in cohesive soils based on finite element analysis. International Journal for Numerical and Analytical Methods in Geomechanics, 38(15), 1541-1555.

Andersen, K. H., J. D. Murff, M. F. Randolph, E. C. Clukey, C. T. Erbrich, H. P. Jostad, B. Hansen, C. Aubeny, P. Sharma, and C. Supachawarote. "Suction anchors for deepwater applications." In International Symposium on Frontiers in Offshore Geotechnics, pp. 3-30. 2005.

Aubeny, C. P., Murf, J. D., & Moon, S. K. (2001). Lateral undrained resistance of suction caisson anchors. International Journal of Offshore and Polar Engineering, 11(03).

Aubeny, C., & Murff, J. D. (2005). Simplified limit solutions for the capacity of suction anchors under undrained conditions. Ocean engineering, 32(7), 864-877.

Bransby, M. F., & Randolph, M. F. (1998). Combined loading of skirted foundations. Géotechnique, 48(5), 637-55.

Byrne, B. W., & Houlsby, G. T. (2003). Foundations for offshore wind turbines. Philosophical Transactions of the Royal Society of London A: Mathematical, Physical and Engineering Sciences, 361(1813), 2909-2930.

Gerolymos, N., & Gazetas, G. (2006). Development of Winkler model for static and dynamic response of caisson foundations with soil and interface nonlinearities. Soil Dynamics and Earthquake Engineering, 26(5), 363-376.

Gerolymos, N., & Gazetas, G. (2006). Winkler model for lateral response of rigid caisson foundations in linear soil. Soil Dynamics and Earthquake Engineering, 26(5), 347-361.

Grajales, F. (2017). Undrained capacity and stiffness of short suction caissons for offshores structures on cohesive soils, Ph.D. Dissertation, Texas A&M University, 2017.

Houlsby, G. T., Kelly, R. B., Huxtable, J., & Byrne, B. W. (2005). Field trials of suction caissons in clay for offshore wind turbine foundations. Géotechnique, 55(4), 287-296.

House, A. R., & Randolph, M. F. (2001, January). Installation and pull-out capacity of stiffened suction caissons in cohesive sediments. In The Eleventh International Offshore and Polar Engineering Conference. International Society of Offshore and Polar Engineers.

Housner, G. W., & Vreeland Jr, T. (1965). The analysis of stress and deformation. California Institute of Technology.

Luke, A. M., Rauch, A. F., Olson, R. E., & Mecham, E. C. (2005). Components of suction caisson capacity measured in axial pullout tests. Ocean Engineering, 32(7), 878-891.

Murali, M., Grajales, F., Beemer, R. D., Biscontin, G., & Aubeny, C. (2015, May). Centrifuge and Numerical Modeling of Monopiles for Offshore Wind Towers Installed in Clay. In ASME 2015 34th International Conference on Ocean, Offshore and Arctic Engineering (pp. V001T10A007-V001T10A007). American Society of Mechanical Engineers.

Schneider, J. A., & Senders, M. (2010). Foundation design: A comparison of oil and gas platforms with offshore wind turbines. Marine Technology Society Journal, 44(1), 32-51.

Sukumaran, B., McCarron, W. O., Jeanjean, P., & Abouseeda, H. (1999). Efficient finite element techniques for limit analysis of suction caissons under lateral loads. Computers and Geotechnics, 24(2), 89-107.

Zhang, Y. (2016). Finite element analysis of elastic behavior of suction caisson, Ph.D. Dissertation, Texas A&M University, 2016.